Energy & Environmental Science

RSC Publishing

PERSPECTIVE

View Article Online
View Journal | View Issue

Cite this: *Energy Environ. Sci.*, 2013, **6**, 1443

Highly efficient dye-sensitized solar cells: progress and future challenges

Shufang Zhang, Xudong Yang, Youhei Numata and Liyuan Han*

Received 21st December 2012
Accepted 11th February 2013

DOI: 10.1039/c3ee24453a

www.rsc.org/ees

High energy conversion efficiency is one of the most important keys to the commercialization of dye-sensitized solar cells (DSCs) in the huge electricity generation market. According to our experience in the persistent efforts that helped to achieve high efficiency DSCs, we selectively review the major progress of improving the energy conversion efficiency of DSCs which may be useful for future applications. We start the discussion from modelling the device by macroscopic equivalent circuit and then highlight some approaches to improve the device performance, such as the molecular engineering of novel dye sensitizers and light trapping effect, tuning the potential of redox shuttles and surface passivation of photoelectrodes, and optimizing the resistance. Finally, we illustrate a roadmap of possible future directions of DSCs with the challenges of how to further improve the efficiency to accelerate the progress in the commercialization of DSCs.

Broader context

Converting solar energy directly into electricity as a clean and renewable energy resource is immensely important to solve the energy crisis and environmental pollution problems induced by the consumption of fossil fuels. In recent years, dye-sensitized solar cells (DSCs) made from low cost materials with environmentally friendly characteristics have shown great potential as alternatives to traditional silicon solar cells. However, the commercialization of DSCs is still being postponed by their relatively lower efficiency. In addition, the slow progress in the improvement of efficiency is unable to match the exponential increase of devoted academic research efforts. In this perspective, with the purpose to accelerate the progress in the commercialization of DSCs, we selectively review some of the major achievements concerned with a further increase of efficiency. Starting from the analysis of the device performance by modelling with a macroscopic equivalent circuit, we point out the approaches that could enhance the efficiency according to our experience in the persistent efforts to develop highly efficient DSCs, which is expected to inspire valuable innovations that will facilitate the commercial application of DSCs.

1 Introduction

Increasing global energy and environmental challenges demand clean and sustainable energy sources to support the activities of modern society. One of the most feasible technologies is to convert solar energy directly into electricity by solar cells. As the alternatives to conventional silicon-based solar cells, dye-sensitized solar cells (DSCs) attract great research interests because of low manufacturing cost and environmentally friendly character.[1–6] Typically, a DSC comprises a transparent conducting oxide (TCO) electrode, a dye-sensitized nanocrystalline titanium dioxide (TiO_2) film, a platinum (Pt) counter electrode, and an electrolyte containing iodide (I^-)/tri-iodide (I_3^-) redox couple between the electrodes (Fig. 1). The major energy conversion processes in DSCs can be described as the following. Solar light is harvested by dye molecules adsorbed on the TiO_2 film. Photo-excited dye molecules inject electrons into the conduction band of the TiO_2 film. Electrons are then

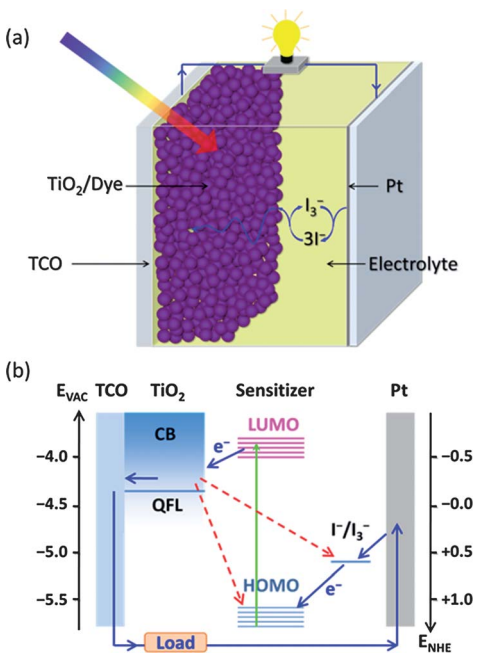

Fig. 1 (a) Schematic structure and (b) main processes in dye-sensitized solar cells.

Photovoltaic Materials Unit, National Institute for Materials Science, Tsukuba, Ibaraki 305-0047, Japan. E-mail: HAN.liyuan@nims.go.jp; Fax: +81 298592304; Tel: +81 298592747

transported toward the TCO front electrode and external circuit. Oxidized dyes are regenerated to neutral state by I^- in the electrolyte and I^- is reproduced by the reduction of I_3^- with electrons from the Pt counter electrode.[7,8] The energy conversion efficiency, η, is determined by measuring the current–voltage (I–V) characteristic parameters, short circuit current (I_{SC}) or short circuit current density (J_{SC}), open circuit voltage (V_{OC}), fill factor (FF), when the test DSC is under solar light irradiation with the power intensity of P_{in} and illuminated cell area of A_{cell}, as given by:

$$\eta = \frac{I_{SC} V_{OC} FF}{P_{in} A_{cell}} \quad (1)$$

Since nano-crystalline DSCs were reported in 1991, numerous research attempts have been made to further improve the energy conversion efficiency for practical applications. Unfortunately, the certified efficiency is still under 12% even though thousands of research papers had been published in the past 20 years.[9] Academic doubts were raised on whether the efficiency of DSCs could be improved highly enough through current research strategies to compete with other solar cells.[10] In addition, although great industrial interests have emerged with the quickly developed technology and equipment by companies such as Sharp, Fujikura, Dyesol, G24i, and Solaronix, the relatively lower efficiency will enhance the entire cost of the practical application including the manufacture, assembly and transport of larger area DSCs modules. This is also the major reason why thin film silicon solar cells failed as a commercialized substitute for fossil fuels in the huge electricity generation market. In contrast to the theoretical performance and the achieved best values in different kinds of solar cells,[9] the DSC with the certified highest efficiency performed relatively lower in terms of J_{SC}, V_{OC}, and FF (Fig. 2). This indicates there is a large space for the improvement of DSCs performance by more effective research. Therefore, the fundamental understanding of the underlying mechanism in DSCs and applicable innovations of materials and structures is highly desired.

A powerful tool for analysing the whole device performance of a DSC is the equivalent circuit modelling, combined with the techniques of frequency-domain methods, such as electrochemical impedance spectroscopy (EIS), intensity-modulated photovoltage spectroscopy (IMVS), and intensity modulated photocurrent spectroscopy (IMPS), and time-domain approaches, such as charge extraction (CE), transient-photocurrent decay

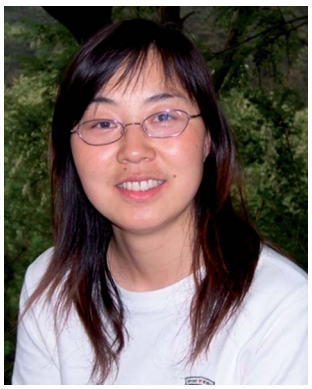

Dr Shufang Zhang received her PhD degree from the Chinese Academy of Sciences in 2008. She worked as a postdoctoral researcher at Tokyo Institute of Technology, and then joined the National Institute for Materials Science (NIMS), Japan in 2009. Her current research interests cover electrochemical analysis of optoelectronic devices and mechanisms understanding interfacial interactions in dye-sensitized solar cells.

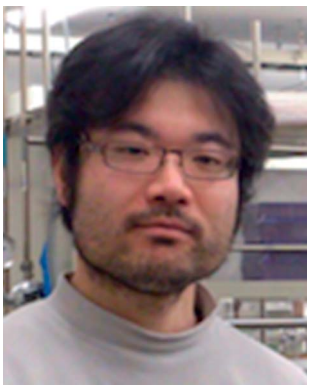

Dr Youhei Numata obtained his PhD degree from the Graduate University for Advanced Studies (Japan) in 2007. He worked as a postdoctoral researcher at RIKEN and then joined the National Institute for Materials Science (NIMS) in 2009. His current interests are the development of new pure-organic and metal–organic complex based photosensitizers, elucidation of their molecular and electronic structure–photovoltaic property relationships, and application in dye-sensitized solar cells.

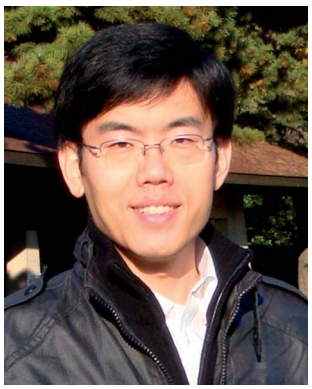

Dr Xudong Yang obtained his PhD degree from the Chinese Academy of Sciences. He worked as a postdoctoral fellow at the University of Cambridge, UK, and then joined in the International Center for Young Scientists of the National Institute for Materials Science, Japan. His current research is focused mainly on understanding the mechanisms of the generation, separation, transport and recombination of excited states in semiconductors, organic materials and optoelectronic devices for the applications in energy conversion.

Dr Liyuan Han is the director of the Photovoltaic Materials Unit, National Institute for Materials Science. After obtaining his PhD from the University of Osaka Prefecture, he worked on dye-sensitized solar cells at SHARP Corporation for 12 years and moved to his current position in 2008. His current research is focused on dye-sensitized solar cells, organic solar cells, and quantum dot solar cells. He is also an inventor with about 100 patents and author in ca. *100 scientific publications.*

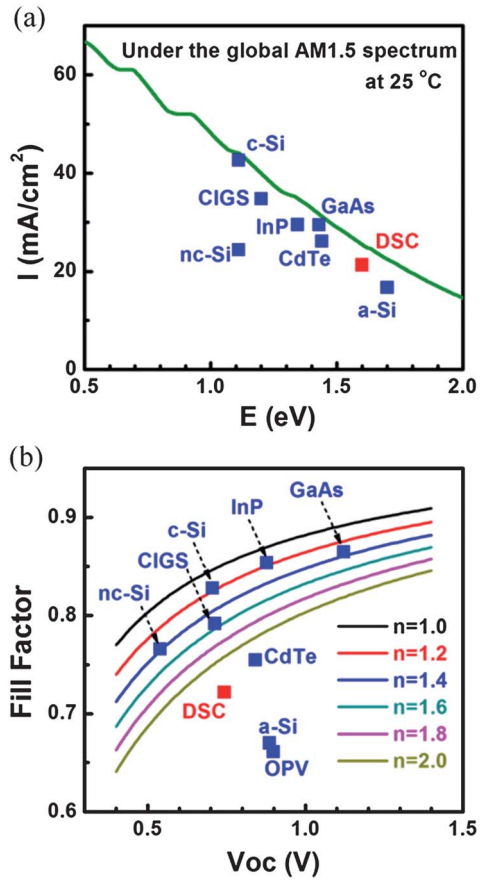

Fig. 2 (a) The theoretic maximum of photocurrent density as a function of the energy gap (solid line) and (b) the fill factor as an empirical function of the open-circuit voltage (solid line) according to the value of the ideality factor, *n*. The solid points are values in different kinds of solar cells that had been certified to obtain the highest efficiency.[9]

(TCD) and transient-photovoltage decay (TVD).[11–15] For understanding the electrochemical mechanisms in DSCs, equivalent circuits consisting of meso/microscopic units have been developed.[16,17] On the other hand, macroscopic equivalent circuits have progressed much to analyse the whole device performance directly.[18,19] The macroscopic models have relatively few parameters to be analysed and show advantages in the attempts to improve the efficiency of not only DSCs but also traditional silicon solar cells.

Fig. 3 represents one example of the equivalent circuit of DSCs which is useful in a high efficiency DSC.[18,20] It includes a diode to represent the electron transfer at the TiO_2–dye–electrolyte interface. C_1 and R_1 are attributed to the redox reaction at the Pt counter electrode; C_3 and R_3 relate to the carrier transport by ions within the electrolyte; R_h is influenced by the sheet resistance of TCO and the contact resistance between the TCO and TiO_2; R_{sh} is the resistance to the back electron transfer across the TiO_2–dye–electrolyte junction.

The current–voltage characteristics of this equivalent circuit under direct current condition are described as:

$$I = I_{ph} - I_0\left\{\exp\left(\frac{q(V+IR_s)}{nkT}\right) - 1\right\} - \frac{V+IR_s}{R_{sh}} \qquad (2)$$

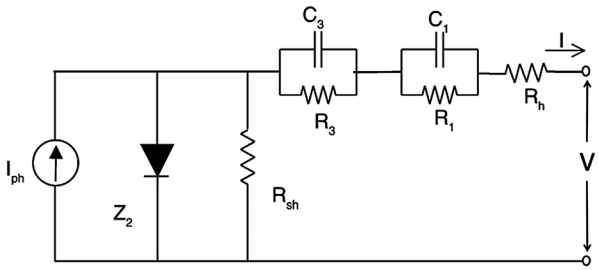

Fig. 3 Example of an equivalent circuit used to analyse and improve the device performance of high efficiency DSCs.[20] Reprinted from ref. 20. Copyright 2006, with permission from Elsevier.

where I_{ph} is the photo generated current, I_0 is diode saturation current, n is the diode ideality factor, k is the Boltzmann constant, T is temperature, R_s is the series resistance and $R_s = R_1 + R_3 + R_h$.

From this equivalent circuit model, the major effect of the components in eqn (2) on the *I–V* characteristic parameters of I_{SC}, V_{OC}, and FF can be analysed. For example at the open circuit condition, V_{OC} is determined by the conditions that the current source I_{ph} is equal to the sum of the current through the diode and the shunt resistance. A small I_0 and large R_{sh} are preferred for a higher V_{OC} under a constant I_{ph}, which can be achieved by many attempts of blocking the electron back transfer at the surface of TiO_2 with a surface coating of organic molecules or large band gap metal oxide.

Benefiting from many excellent reviews on DSCs, scientific researches on novel component materials and underlying mechanisms have been developed rapidly in recent years. However, as the total efficiency grows slowly in contrast to the exponentially increased research efforts, doubts on whether the efficiency of DSCs could achieve high enough to compete with other solar cells were raised. In this perspective article, we selectively review the major progress of improving the energy conversion efficiency of DSCs which may be useful for future applications. We highlight some approaches to increase J_{SC} by molecular engineering novel sensitizers and light trapping effect, V_{OC} by tuning potentials and surface passivation, and FF by optimizing the resistance. Finally we propose a roadmap of possible future directions, with the challenges of how to further improve the efficiency of DSCs. Although we cannot include all of interesting findings due to limitation of article length, we hope the present perspective article is helpful for researchers in accelerating the progress of highly efficient DSCs.

2 Improvement of DSCs

2.1 Short circuit current

At short circuit the photo-generated charges are expected to flow into the external circuit with unit efficiency. According to the equivalent circuit (Fig. 3), the short circuit current, I_{SC}, is equal to the difference between the photo-generated current I_{ph} and that lost in the diode and shunt resistance. When a DSC is under the illumination with the incident photon flux of $I_{photon}(\lambda)$, the total current flowing in the external circuit is then expressed as:

$$I_{sc} = q_e \int_{\lambda_{min}}^{\lambda_{max}} I_{photon}(\lambda)\mathrm{IPCE}(\lambda)\mathrm{d}\lambda \quad (3)$$

where q_e is the electron charge and IPCE(λ) is defined as the incident monochromatic photon-to-electron conversion efficiency, as given by:

$$\mathrm{IPCE}(\lambda) = \eta_{LHE}\eta_{inj}\eta_{cc} \quad (4)$$

where η_{LHE} is the light harvesting efficiency, η_{inj} is the electron injection yield from the photo-excited dye into TiO_2, and η_{cc} is the charge collection efficiency at the electrodes. Practically, it was confirmed that η_{inj} with unit efficiency requires approximately 0.2 V of over-potential ($-\Delta G$) between the TiO_2 conduction band (CB) and the dye lowest unoccupied molecular orbital (LUMO) level,[21] and 0.3 V of $-\Delta G$ between the dye highest occupied molecular orbital (HOMO) level and redox potential for sufficient driving forces of electron injection from the dye to the CB of TiO_2 and the regeneration of oxidized dye,[22,23] respectively. In present high efficiency DSCs with efficiency over 10%, the production of η_{inj} and η_{cc} have been found to be close to 1.[5] Therefore the major strategy to increase the short circuit current, I_{SC}, is to improve the light harvesting efficiency, η_{LHE}, which depends on the molar extinction coefficient (ε) of the dye, the amount of dyes anchored on TiO_2 film, and the optical path length of incident light within the dye-sensitized film.

Finding dyes with intense ε in both the visible and the near-IR (NIR) regions is essentially required in order to efficiently absorb more solar light and obtain higher photocurrent. For example, Fig. 4 shows the solar light spectrum and obtained photocurrent calculated from eqn (3) with an assumed IPCE of 100% integrated from the UV region to the band edge of the sensitizer. When the IPCE onset is 800 nm, J_{SC} value is 27.3 mA cm^{-2}. If IPCE onset expanded to 920 nm, the photocurrent can be obtained up to 34.7 mA cm^{-2}. In order to achieve a broad light harvesting spectrum, narrowing the band gap between the HOMO and the LUMO of the sensitizer molecule is required. In addition, with the increase of the thickness of TiO_2 film, the charge recombination between the electron in the TiO_2 film and redox mediator will increase and then V_{OC} will decrease. Therefore, it is necessary to decrease the thickness of the TiO_2 film and consequently the amount of anchored dye is also decreased. Intense ε is thus required for strong light harvesting in a thinner TiO_2 film and this can improve not only J_{SC} but also V_{OC} at the same time.

2.1.1 Molecular engineering on dye sensitizers. Up to now, many types of compounds have been developed as sensitizers, such as metal–organic complexes, metal-free organic compounds, Zn porphyrins, and Zn phthalocyanines. For application in highly efficient DSCs, some basic structural features are required, such as the HOMO–LUMO should be suitably spatially separated and the anchoring group must be bound to the electron acceptor part of the molecular structure (usually by coordination bonding) for stabilization of the photo-excited state, efficient injection of the generated electrons into TiO_2 electrode, efficiently regeneration of oxidized dyes, and suppression of the electron back reactions. Here, we review recent progress in different types of dye sensitizers in DSCs, with specific emphases on the strategies of molecular design and corresponding effects on the cell performance.

2.1.1.1 Ru polypyridyl complex. Ru polypyridyl dyes, the most successful sensitizers in DSCs, exhibit superior performances owing to the broad light absorption capability expanding to the NIR region, appropriate HOMO and LUMO energy levels applying to the TiO_2–iodide system, a long-lived photo-excited state, high molecular stability, and rich structural variation. In these Ru polypyridyl complexes, the HOMO is mainly localized on the Ru and electron donating ligands, and the LUMO is mainly distributed over the polypyridyl ligand (Fig. 5). The distribution of LUMO and HOMO is favorable for efficient electron injection into TiO_2 *via* chemical bonding and the regeneration of oxidized dyes.

Generally, Ru polypyridyl complexes show prominent absorption peaks at the UV region and the visible-NIR region, respectively. The absorption band appears in the visible-NIR region is assigned as singlet to singlet metal-to-ligand charge transfer (^{1}MLCT) from Ru to the polypyridyl ligand. The expansion of π-conjugation of polypyridyl ligand will lead to a decrease of the LUMO energy level and result in a bathochromic shift of the absorption band. For example, the structure difference between N719 dye[24] and black dye[25] is replacing the two 4,4′-dicarboxyl-2,2′-bipyridyl (dcbpy) ligands in N719 with one 4,4′,4″-tricarboxyl-2,2′:6′,2″-terpyridyl (tctpy) ligand and one NCS ligand in the structure of black dye. The significant shift of the ^{1}MLCT band of about 530 to around 610 nm can be attributed to the wide π-conjugation in the tctpy ligand and strong

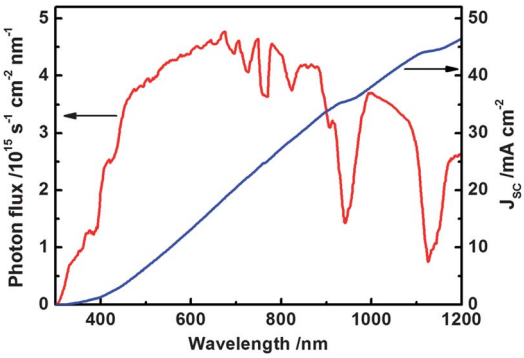

Fig. 4 Solar light spectrum (red) and calculated photocurrent (blue) from eqn (3) with an assumed IPCE of 100% integrated from 300 nm to the corresponding wavelength.

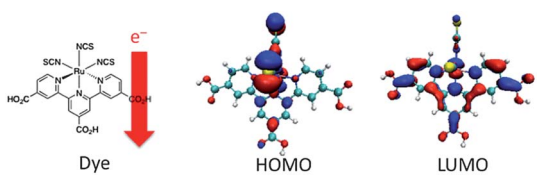

Fig. 5 Electron flow and the HOMO and LUMO distributions of black dye (N749).

electron-donating properties of the three NCS ligands (Fig. 6). Correspondingly, the IPCE onset of DSC is bathochromatically shifted from *ca.* 800 (N719) to over 900 nm (black dye), as shown in Fig. 6. By further π-expansion of the polypyridyl ligand (in N719) to 2,2′:6′,2″:6″,2‴-quaterpyridine (qpy) (in N886), the ^{1}MLCT band was bathochromically shifted to 637 nm. While, the η_{inj} was deteriorated due to the dye-aggregation problem (*vide infra*).[26]

Additionally, exchange of the central metal atom is also an effective way to drastically change absorption property of the sensitizer. As a successful case, some Os tctpy dyes have been reported.[27–29] For the Os tctpy dyes, both enhancement of ε of the ^{1}MLCT and ^{3}MLCT bands occurred in the NIR region due to the energy level shift and heavy atom effect of the Os ion. As a result, the absorption spectrum was expanded to *ca.* 900 nm and the IPCE onset was extended to 1000 nm.

For the Ru polypyridyl dyes, despite the wide spectral coverage from the UV to the NIR region, the molar extinction coefficient of the MLCT band in visible-NIR spectral region is generally lower compared with those of organic dyes. For example, ε values of N719 and black dye at λ_{max} of ^{1}MLCT are approximately 14 700 and 7000 M^{-1} cm^{-1}, respectively (for organic dyes, 15 000–60 000 M^{-1} cm^{-1}). Therefore, in order to sufficiently absorb the photons in the NIR region, a thick TiO_2 film is needed. As mentioned above, increase of the TiO_2 thickness decreases the V_{OC} value; therefore, increase of the ε of the Ru polypyridyl dye is an important way to improve the cell performances. In order to enhance the extinction coefficient of the Ru dyes, introduction of the π-conjugations into the co-ligand or polypyridyl ligand was carried out.

In 2006, a new heteroleptic Ru dye, N945H was reported, in which one bpy ligand is substituted by two electron-donating 2,5-dimethoxystyryl groups (Fig. 7a).[30] Its ε value of ^{1}MLCT band was successfully increased (18 900 M^{-1} cm^{-1}) compared with that of N719 dye. It was revealed that spatial separation of electron-donating substituents from the TiO_2 electrode is important for the molecular design of Ru polypyridyl dye to achieve high efficiency by detailed DFT calculation. Instead of the styryl groups, more electron-rich heteroaromatics such as thiophene and furan were introduced owing to the higher electron density and molecular stability.[31–36] Heteroleptic Ru dyes, C101 and C106 possessing thiophene derivatives with hexyl chains on the bpy ligand achieved not only high conversion efficiency of over 11% but also high device durability.[30,35] In these cases, the HOMO energy level was elevated with increasing the electron-donating property of the π-conjugates. Additionally, such long alkyl chains can suppress dye aggregations, and improve the V_{OC} and η_{inj} as discussed in Section 2.1.1.2.[37]

Furthermore, the π-expansion concept was also applied to the Ru tpy complexes (Fig. 7b and c), because the improvement of the ε value is a more important challenge for the Ru tpy dyes owing to their lower ε values. Exchanges of the NCS of the black dye for the electron-donating π-conjugated ligand were carried out as well as for Ru bpy dyes.[38–40] On these sensitizers, ε values of the ^{1}MLCT band were increased, but λ_{max} were unfortunately blue-shifted compared with that of the black dye due to the difference in σ-donor and π-acceptor properties between the alternative and NCS ligands. On the other hand, development of the tpy ligand of black dye analogues with the π-expansion concept was recently reported.[41–43] The ε of these dyes in the UV-visible region were successfully enhanced. While, the

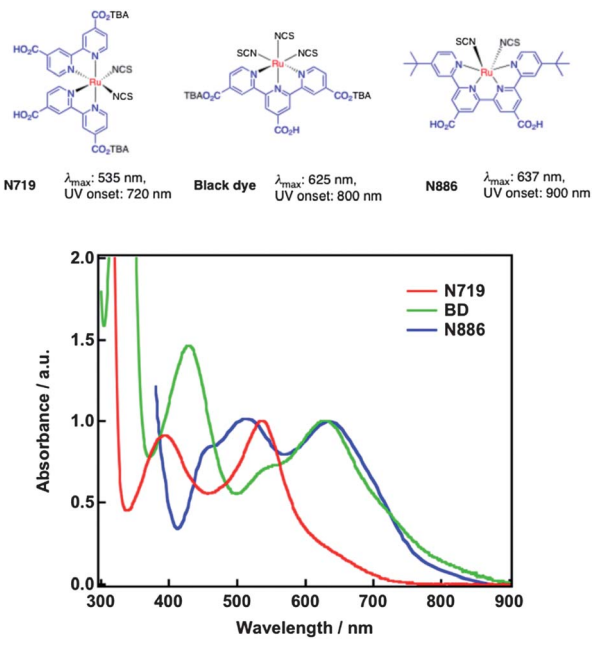

Fig. 6 Molecular structures and normalized absorption spectra (by ^{1}MLCT bands) of Ru–NCS_x–polypyridyl (red: N719 dye, green: black dye, and blue: N886).

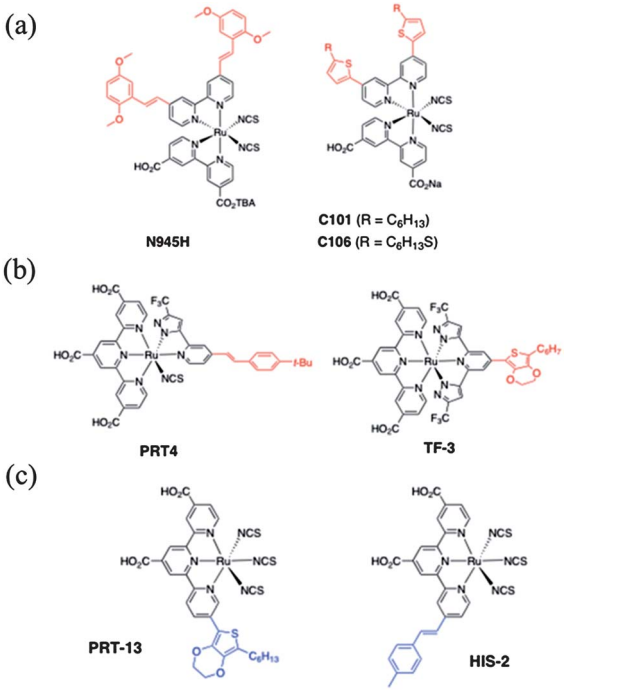

Fig. 7 (a) Molecular structures of the Ru-bpy sensitizers with π-conjugate system, N945H,[30] C101,[31] and C106,[35] (b) donor substituted,[42,78] and (c) tpy substituted black dye analogues.[43,44]

ε values of the ^{1}MLCT band were almost unchanged in comparing with those of black dye. In these cases, one carboxylate of tctpy ligand was replaced by the π-conjugation on 5- or 6-position of the pyridine ring. DFT calculations revealed that when carboxylate was substituted by hexylthiophene or other strong donor moieties, the low energy LUMOs were mainly distributed on the dctpy ligand.[41,42] Recently, a Ru dctpy dye, HIS-2 bearing 4-methylstyryl moiety on the 4-position of the pyridyl ring was developed.[44] The low energy LUMOs of HIS-2 dye are distributed over dctpy and styryl moieties. As a result, the ε values of not only the n–π and π–π* transitions in UV region but also ^{1}MLCT band in NIR region were enhanced. The IPCE spectrum of HIS-2 was improved in all spectral region compared with that of black dye. The difference in the LUMO distribution among these Ru dctpy dyes may be attributed to the substitution position and electron-donating properties of the substituent.

From a viewpoint of molecular stability, development of alternative multidentate ligands of NCS is significantly important, because the monodentate NCS is easily eliminated or exchanged for solvent, redox mediator, and/or additives in the electrolyte under illuminated condition. A cyclometalated Ru complex, YE-05 was firstly reported as a "NCS-free" Ru dye with a conversion efficiency of 10.1%.[45] Consequently, various NCS-free Ru dcbpy[45–48] and Ru tctpy[40,42] sensitizers were developed and showed conversion efficiencies of over 9%.

2.1.1.2 Metal-free organic dyes. Metal-free pure organic dyes are also promising candidates as sensitizers in DSCs due to the high molecular extinction coefficient, low cost, rare metal free, and high design flexibility of the molecules. Almost all of the organic dyes are designed based on donor–π spacer–acceptor (D–π–A) architecture, in which the donor and acceptor parts are combined with the π-spacer and the anchoring group is attached with the acceptor part as shown in Fig. 8. Typically, as donor parts, electron-rich moieties such as triarylamines,[49] carbazoles,[50] indolines,[51–54] phenoxazines,[55–57] dithienothiophenes[58] are often employed. Counterpart acceptor parts are composed of an electron-withdrawing unit and an anchoring group. Practically, cyanoacrylic acid and its analogues,[59,60] rhodanines,[51,52,55,61–63] and pyridines[64,65] are frequently used owing to their electron-withdrawing properties and coordinating features to the TiO_2 electrode. As π-spacer units, π-conjugated systems such as polyenes,[66–68] polyynes,[69–71] thiophenes,[72–75] furanes,[76–78] pyrroles,[79–81] fused thiophenes,[82–85] diketopyrrolopyrrole,[86–88] benzothiadiazole,[53,54,89,90] and benzotriazole[91,92] are incorporated into D–π–A dyes. In a D–π–A organic dye, the HOMO is mainly localized at the donor and the electron-rich π-spacer part, and the LUMO is distributed on the acceptor part and the anchoring group. Generally, the D–π–A dyes show sharp and intense absorption in the visible-NIR region, in contrast with Ru polypyridyl dyes. Therefore, in organic dyes, bathochromic shift and an increase of the number of the absorption bands have been attempted to improve the conversion efficiency. In the D–π–A type organic dyes, modification and exchange of the donor, π-spacer, and acceptor parts, and π-expansion are the main strategies to control their frontier energy levels and enhance the molecular extinction coefficient.

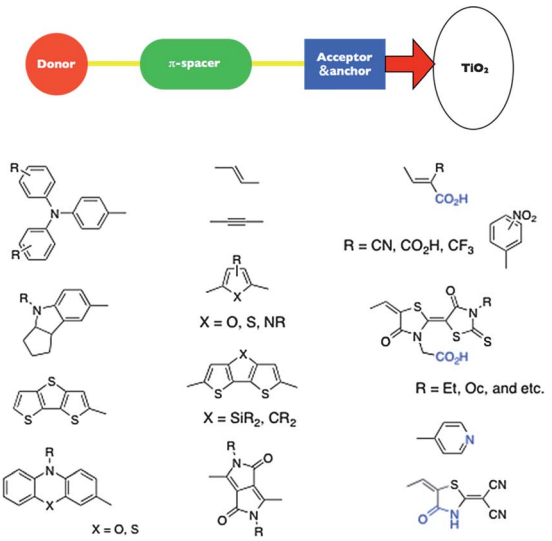

Fig. 8 Schematic drawing of D–π–A type organic dye and some samples of the donor, π-spacer and acceptor with anchoring (in blue) components.

The HOMO and LUMO energy levels are dominated by the energy levels of the donor and acceptor moieties, and the conjugation length of the π-spacer. For instance, the HOMO energy level of the dye was elevated when replacing triphenylamine (TPA) at the donor part by the stronger electron-donating indoline moiety.[78] On the other hand, expansion of the π-system, substitution of the thiophene π-spacer with wider π-spacers such as thienothiophene and dithienothiophene or increasing the thiophene unit number, can enhance ε and cause a bathocromic shift of the absorptions.[74,93–95] In the case of typical TPA–oligothiophene–cyanoacrylic acid based dyes, increasing of the number of the thiophene and vinyl moieties in the π-spacer, bathochromic shift and increase of extinction coefficient of the charge transfer (CT) band occurred, as shown in Fig. 9. In addition, planarity of the π-conjugation system also affects the position of λ_{max} and ε of the D–π–A sensitizers. In comparison with the planarity phenyl-furan π-spacer, dye with twisted configuration spacer of biphenyl exhibited blue-shift and decrease of ε due to less overlapping of π-orbitals.[78] In the case of ethylene as spacers, increasing the number of adjacent ethylenes leads to an increase of ε and a bathochromic shift of the absorption band while a decrease in the IPCE is attributed to the dye-aggregation and photoiosmerization.[96,97] Until now, among the reported D–π–A type metal-free organic sensitizers, the highest conversion efficiencies of DSCs based on this kind of dye are about 10%.[82,98–103]

As another type of organic dye, zwitterion-based NIR organic sensitizers such as squaraine,[104–111] cyanine,[112–116] and related compounds[81,117–121] have been also reported. These NIR dyes exhibit very intense CT bands (ε = 100 000–200 000 M^{-1} cm^{-1}) at λ_{max} = 600–800 nm. From the very early period of DSC research, such NIR dyes have been studied as sensitizers in the DSCs. However, only poor efficiencies were reported due to the inappropriate HOMO and LUMO energy levels, symmetric structure, lack of conjugation of anchoring groups, and dye aggregations. For the squaraine dyes, firstly a symmetric

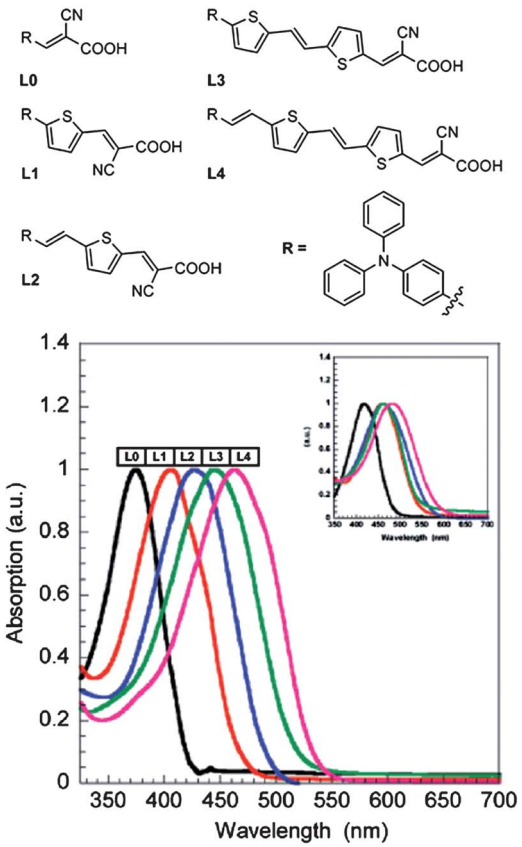

Fig. 9 Normalized absorption spectra of the L0–L4 dyes in acetonitrile solution upon addition of TBAOH. Inset: normalized absorption spectra of the L0–L4 dyes in a plain acetonitrile solution. (Right) Normalized absorption spectra of the L0–L4 dyes adsorbed onto TiO_2.[74] Adapted from ref. 74, reprinted with permission from Elsevier.

structure was employed (Sq 04).[105] After introduction of an asymmetric (push–pull type) molecular design, although the CT bands of the asymmetric dyes were slightly blue-shifted compared with those of symmetric dyes due to the LUMO localization on the anchoring groups, electron injection efficiencies and overall conversion efficiencies of DSCs were further improved (Sq 01).[107] However, problems of low V_{OC} due to the charge recombination and lack of absorption from the UV-to-visible region have still remained. YR6 dye based on the combination of the squaraine unit with π-spacer and strong electron-withdrawing cyanoacrylic acid anchor improved V_{OC} and compensated the lack of absorption from the UV-to-visible region, achieving near ideal panchromatic sensitization by pure organic dye.[110]

Dye-aggregation problems seriously deteriorate electron injection efficiency in the DSCs due to the intermolecular energy and/or electron transfer (ET) *via* the intermolecular π–π and columbic interactions. As one solution, co-adsorption of deoxycholic acid (DCA) with dye molecule is often employed. For example, black dye highly aggregates in the DSC and the η_{inj} is decreased. By co-adsorption with DCA, the conversion efficiency is drastically improved. However, the co-adsorption method requires cumbersome optimizations for each dye. Therefore, it is very necessary to find an efficient and convenient strategy to suppress the dye-aggregation on the TiO_2 surface. The introduction of long or bulky substituents into the dye skeleton is an efficient way. MK-2 dye bearing *n*-hexyl chains on the thiophene spacer showed better electron injection efficiencies and higher V_{OC} values than that of MK-3 dye without alkyl chains (V_{OC} of MK-2 and MK-3 are 0.72 and 0.64 V, respectively) during the immersion process without co-adsorbent, even though the π-conjugation of MK-2 is wider than MK-3 (Fig. 10a).[75] The introduction of twisting into π-spacers is another efficient way to suppress the intermolecular ET owing to lesser intermolecular interactions, even if the π-conjugations are expanded. As shown in Fig. 10b, planar D-2 dye tends to aggregate on the TiO_2 surface and showed low IPCE values. In contrast, twisting D-1 dye efficiently suppressed the dye-aggregation even without co-adsorbent, and the IPCE maximum reached up to 80%.[122]

2.1.1.3 Zn porphyrin and phthalocyanine dyes. Macrocycles such as Zinc(II)-porphyrins (ZnPor) and Zinc(II)-phthalocyanines (ZnPc) are also very promising candidates as NIR sensitizers to be applied in DSCs. The ZnPor and ZnPc dyes generally exhibit a Soret-band and Q-band at around 400–500 nm and at around 500–700 nm, respectively, in their absorption spectra. They possess outstanding molecular stability, appropriate frontier orbital energy levels for efficient electron injection into the

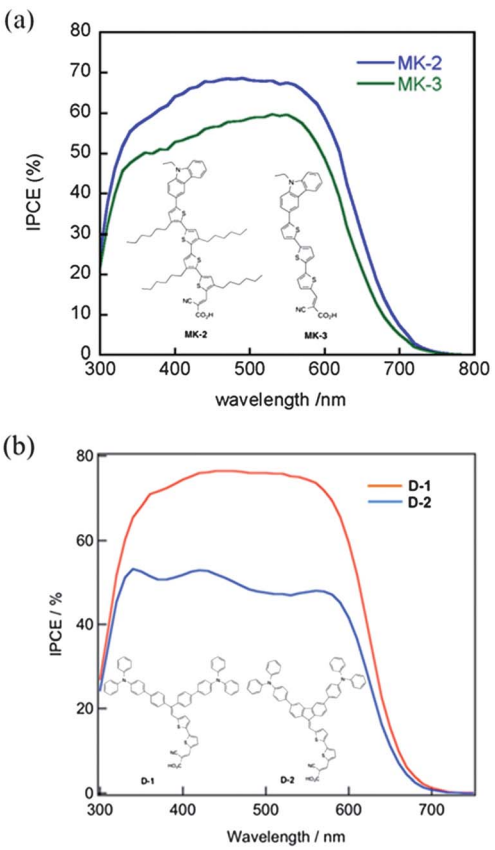

Fig. 10 Molecular structures and IPCE spectra of (a) MK-2 and MK-3,[75] and (b) D-1 and D-2.[122] Adapted from ref. 75, Copyright 2007, with permission from American Chemical Society.

conduction band of TiO_2 film and oxidized dye regenerations, and structural versatility for fine-tuning of energy levels. However, they have common problems in applications as efficient sensitizers for DSCs: (1) owing to the wide and planar π-conjugated molecular structure, they tend to aggregate each other even in the solution which can lead to unfavorable charge recombination; (2) because both the HOMO and LUMO are localized in the macrocycles, it is difficult to bring photo-excited electrons out from the macrocycle and inject into the TiO_2; (3) essentially ZnPors and ZnPcs do not absorb between the Soret- and Q-bands in the visible region. Accordingly, development of the ZnPors and ZnPcs has been promoted to overcome these problems.

ZnPor dyes show very intense and sharp Soret bands (ε larger than 100 000 M^{-1} cm^{-1}) at around 450 nm and moderate Q-bands (ε larger than 20 000 M^{-1} cm^{-1}) at around 600 nm. Diverse ZnPors can be prepared because the peripheral *meso*- and β-positions of pyrrole ring, and the π-system can be independently and asymmetrically substituted and extended, respectively.[123–125] By introduction of an asymmetric nature into dye design, superior ZnPc dyes were developed (Fig. 11a). In 2007, a push–pull type ZnPor sensitizer, GD2, with *meso*-positions fully substituted by tolyl groups and π-conjugated anchor attached on the β-position was reported.[126] In GD2, the asymmetric molecular structure caused a directional electron flow and efficient electron injection from the LUMO into TiO_2 and achieved a conversion efficiency of 7.1%. In order to separate the HOMO and LUMO spatial distributions more efficiently, strong electron donors and acceptors with anchors were diagonally introduced into the porphyrin core (YD-2).[127] As shown in Fig. 12a, due to the strong electron-donating diphenylamine moiety, the HOMO is mainly localized on the diphenylamine and the LUMO is distributed over the porphyrin core and anchoring group. On the other hand, for the porphyrin dye, dye-aggregation causes a more serious problem on the photovoltaic properties due to the wide and planar porphyrin core. However, for the ZnPors, due to the much wider π-system, the alkylation method described above cannot effectively suppress the aggregation among the porphyrins. Therefore, the development of a new strategy is required. Effective solutions with the introduction of the *ortho*-substituted phenyl ring on *meso*-positions have been reported.[5,128] As shown in Fig. 12b, molecular dynamics calculations of LD dyes revealed that alkyl chains (pink) on the *meso*-phenyl rings effectively enveloped the porphyrin core. With increasing the chain length, IPCEs of the LD dyes based cell were improved. For the LD14 and LD16 substituted with *n*-$C_{12}H_{25}$ chains, the IPCE maxima reached up to 90%.

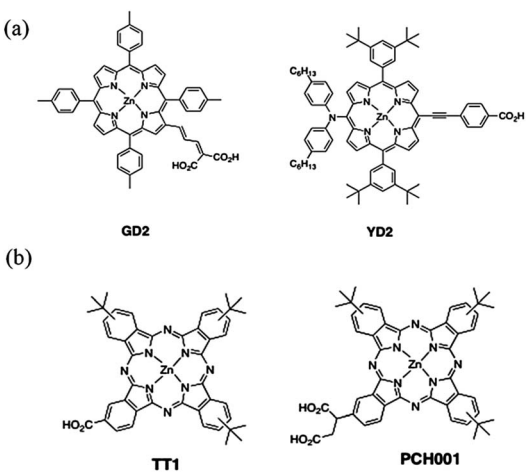

Fig. 11 (a) Molecular structures of asymmetric and D–A type ZnPor dyes; and (b) asymmetric ZnPc dyes.

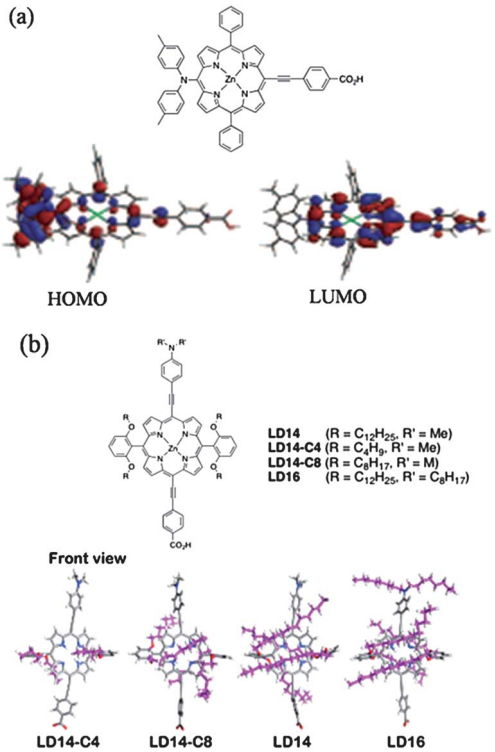

Fig. 12 (a) The HOMO and LUMO distributions of D–A type porphyrin dye; (b) inhibitions of the intermolecular π–π stacking on porphyrins by the long alkyl chains (pink) enveloping the porphyrin core.[132]

In contrast to the various ZnPor dyes applied in DSCs, only few ZnPc dyes have been reported because asymmetric ZnPc dyes are very difficult to be synthesized. The early reported efficiencies with ZnPc dyes were only less than 1%.[129–132] In 2007, new unsymmetrical ZnPc sensitizers, PCH001[133] and TT1,[134] substituted by three electron-donating *t*-Bu groups and one anchoring group were reported with higher conversion efficiencies of 3.05 and 3.52%, respectively (Fig. 11b). Furthermore, important insight on molecular design of ZnPc for suppression of dye-aggregation was reported in 2010.[135] Three ZnPc dyes, PcS2, PcS5, and PcS6 possessing different sizes of substituent on the peripheral positions showed different aggregation properties depending on the bulkiness of the substituent. Increasing the steric hindrance of the peripheral substituent by bulky structures to suppress the intermolecular dye aggregation effectively improved the performance of unsymmetrical ZnPc sensitizers in DSCs. With respect to *t*-Bu group-substituted PcS2 dye, PcS6 substituted with very bulky

2,6-diphenylphenoxy groups produced much higher IPCE with a maximum of 78% and achieved η of 4.6%. Additionally, the efficient synthesis of ZnPc dyes is still limited; therefore, a more elegant way is anticipated to develop ZnPc dyes for higher efficiency.

2.1.2 Co-sensitizers. Ideally, the dye sensitizer in a DSC should absorb all photons above a threshold energy of 1.3–1.4 eV (about 920 nm) under AM 1.5 illumination (power of 100 mW cm^{-2}).[136] Although various types of dyes have been investigated as we have summarized above, it is practically difficult to synthesize a single dye that has high light-harvesting ability covering from the UV to the NIR region and can efficiently inject the photo-generated electron into TiO_2. Therefore, a feasible strategy known as "dye cocktails" by using plural dyes with complementary absorption properties to co-sensitize the TiO_2 film was developed.[126,137–139]

For black dye, one of the most widely used dyes in highly efficient DSCs, the IPCE spectrum covers the entire visible wavelength region and extends into the NIR region. However, there is a dip at around 400 nm which is caused by the competitive absorption of I_3^- in the electrolyte. To further increase the efficiency of DSCs based on black dye, one useful method is filling this dip in IPCE by a co-sensitizer. The co-sensitizer should have three characteristics: (i) strong light absorption ability at this region; (ii) a suitable structure to avoid competitive adsorption and aggregation among dyes; (iii) to reduce the recombination of electrons in the TiO_2 film with I_3^-. A simple D–π–A structured organic dye, Y1, had fulfilled these requirements and successfully recovered the dip in the IPCE spectrum of black dye at around 400 nm, as shown in Fig. 13. A cell co-sensitized with black dye and Y1 significantly improved both J_{SC} and V_{OC}, and achieved a new efficiency record of 11.4%.[6] Other organic dyes such as D131 and NKX-2553 also improved the performance of black dye-based DSCs and achieved a conversion efficiency of over 11.0%.[140,141] Another ruthenium complex C106 and organic dye D131 were selectively distributed on the TiO_2 surface due to their different molecular sizes and anchoring groups and enhanced both J_{SC} and V_{OC} with respect to the individual dyes.[142] For porphyrin dye YD2-*o*-C8, with relatively less absorption in the range from 480 to 630 nm, co-sensitized with Y123 dye with an absorption maximum at 532 nm showed an increase of IPCE in the green spectral region.[5] The combination of a zinc porphyrin dye LD12 with an organic dye CD5 also increased the J_{SC} from 14.97 to 16.74 mA cm^{-2}, contributing to a 12% enhancement of the efficiency.[143] Furthermore, a cell co-sensitized with two porphyrin dyes (YD2-*o*-C8 and YDD6) and an organic dye (CD4) indicated a high IPCE spectrum in the wavelength region of 400–700 nm and extended the spectrum to the near infrared region.[144] In comparison to the great progress by combination of ruthenium dyes or porphyrin dyes with metal-free organic dyes, however, there are only a few achievements in highly efficient DSCs co-sensitized with two or more metal-free organic dyes.[138,145–148]

2.1.3 Light trapping effect. Besides developing dyes with intense light harvesting ability over a broader wavelength range, another effective way for the improvement of light harvesting is to increase the light trapping effect which is also widely used in thin film solar cells. In DSCs, an efficient way to increase the optical path length within TiO_2 films is by adding large diffusive particles into the conventional nano-crystalline TiO_2 layers or adding a scattering layer on the back side of the nano-crystalline TiO_2 layers.[149,150] Fig. 14 shows the effect of particle size of the scattering layer on the IPCE spectrum of a N719 dye sensitized solar cell. The IPCE is effectively increased at the 400–800 nm region by a scattering layer with particle size of 100–300 nm and the IPCE is further increased at the 600–800 nm region when the scattering layer is composed of larger particles with size about 400 nm. As the light absorption of most dyes is much lower in the wavelength region around 800 nm, particles with size of about 400–500 nm are usually used as the scattering centres because incident light can be scattered on the surface of particles with a size half of the light wavelength. However, some results of light-scattering effect to improve the efficiency over 10% were hardly reproduced by other groups,[151,152] although a similar TiO_2 electrode was used, because the effect is also influenced by certain subtle properties of the TiO_2 electrodes,

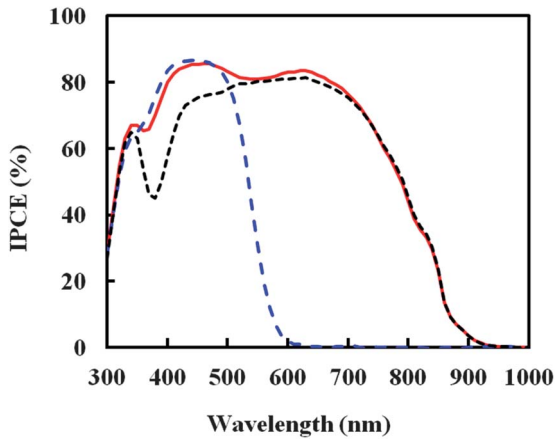

Fig. 13 IPCE spectra of DSCs based on Y1 (blue, dashed line), black dye (black, short dashed line), and Y1 + black dye (red, solid line).[6]

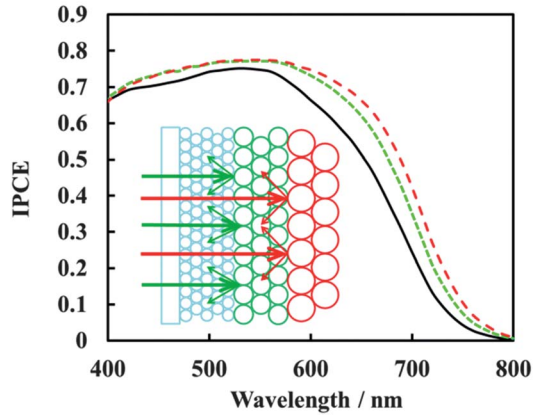

Fig. 14 IPCE spectra of N719 sensitized solar cell with no light scattering layer (black solid line), a scattering layer with particle size of 100–300 nm (green short dashed line), and a scattering layer with particle size of about 400 nm (red dashed line). Inset: schematic pictures of the light-scattering effect with scattering centres or scattering layers.

such as the configuration of TiO_2 particles, the distribution of particle size, the preparation method, and even the sintering conditions.[153,154] In order to evaluate the light scattering effect of TiO_2 films quantitatively, we introduced the concept of haze which is a well-known index of TCO substrates for light scattering in the field of silicon solar cells.[155–157] Haze is defined as the ratio of diffused light to the total light transmitted through the electrodes.[158] This index enabled us to investigate the relationship between the light scattering effect and IPCE spectra at different wavelength regions and further increase the J_{SC}. By systemically controlling the haze, a high J_{SC} of 21 mA cm^{-2} was achieved with the haze factor of 76% at 800 nm.[18,20] This result further demonstrated that the haze of the TiO_2 film is a useful index for improving J_{SC} in DSCs.

Although the most widely utilized light-trapping configuration is the bilayer structure consisting of a transparent underlayer and a scattering layer with large particles, this configuration is still not perfect since less dye adsorption on the scattering layer will increase recombination losses at grain boundaries of particles. In order to simultaneously promote the dye loading and light scattering, recently, much effort has been focused on developing hierarchical TiO_2 nanostructures with multi-function for application as the main layer or scattering layer in the photoelectrodes of DSCs.[159–166] The building units of isotropic morphologies such as spheres, cubes, and polyhedrons (Fig. 15a), linear morphologies such as rods, wires, and tubes (Fig. 15b), or planar morphologies as platelets and sheets (Fig. 15c) for the hierarchical TiO_2 nanostructures have been attempted. For example, mesoporous anatase TiO_2 beads composed of anatase TiO_2 nanocrystals with surface areas of up to 108.0 m^2 g^{-1} and tunable pore sizes from 14.0 to 22.6 nm have been prepared and applied in photoelectrodes of DSCs.[160] With promotion of the light harvesting within the electrodes without sacrificing the accessible surface for dye loading, the conversion efficiency was increased by using these TiO_2 beads in DSCs compared to that of the cell with standard P25 nanoparticles. Another isotropic morphology material, nanoembossed hollow spherical TiO_2 was also prepared and investigated for use in highly efficient DSCs. The walls of the hollow spheres composed of anatase TiO_2 nanocrystalline particles were able to adsorb N719 dye 5 times higher than the normal 400 nm diameter scattering particles with flat surfaces. A bilayer photoelectrode film with a nanocrystalline TiO_2 underlayer and a light-scattering layer comprised of spherical TiO_2 nanorod aggregates with high surface area not only enhanced light scattering but also prolonged exciton lifetime.[167] TiO_2 microplates with uniform hexagonal shape were prepared and demonstrated superior light scattering that can reflect more light back into the photoelectrode. The light harvesting and conversion efficiency of DSCs made by the TiO_2 microplates as the scattering layer were enhanced compared to the commercial scattering TiO_2.[168] Therefore, the main feature of hierarchical photoelectrodes enhances the light scattering or reflection and at the same time the composed nanocrystals provide a large surface area for dye loading. Thus, hierarchical photoelectrodes are highlighted for improvement of the conversion efficiency of DSCs.

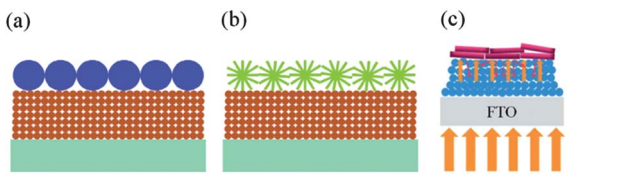

Fig. 15 Schematic pictures of the light-scattering effect caused by different light-scattering layers: (a) large-sized solid particles;[161] (b) spherical TiO_2 nanorod aggregates;[161] (c) TiO_2 microplates.[168] Reprinted from ref. 161. Copyright 2012, with permission from Elsevier.

2.2 Open circuit voltage

Under the open circuit condition, all photo-generated charges are recombined inside the cell. According to the equivalent circuit given in Fig. 2, the photo current I_{ph} equals to the sum of the current through the diode and the shunt resistance. When the device is well designed and the shunt resistance is large enough to limit the current flowing in it to be negligible, the open circuit voltage is deduced from eqn (2) as:

$$V_{OC} = \frac{nkT}{q_e} \ln \frac{I_{ph}}{I_0} \quad (5)$$

I_0 can be obtained by measuring the current–voltage curve under dark and finding the Y-intercept of the log-linear plotted curve at $V = 0$, and the ideality factor, n, is related to the slope. Generally the diode ideality factor, n, has a value between 1 and 2 depending on the non-linear recombination in DSC. The saturation current, I_0, may vary by orders of magnitude depending on the charge recombination in the device, and I_{ph} has a variation depending on the IPCE spectrum as discussed in the previous section. Therefore the major method to improve V_{OC} is to control the saturation current, I_0, which is typically expressed as:

$$I_0 = n_{e0} k_{rec} N_A \quad (6)$$

where n_{e0} is the density of electrons available for recombination in thermal equilibrium when the device is in the dark, k_{rec} is the recombination rate, N_A is the density of electron acceptor of the redox species available for recombination. In this case, electrons are almost trapped and moves by diffusion in the semiconductor, and n_{e0} is:

$$n_{e0} = N_S \exp\left(\frac{E_A - E_{CB}}{\alpha kT}\right) \quad (7)$$

where N_S is the density of the semiconductor conduction band/trap states, E_{CB} and E_A are the energy level of the semiconductor conduction band and redox species (*vs.* vacuum), respectively, and α is the tailing parameter of the exponentially distributed trap states. It can be deduced that the major strategies of improving V_{OC} include the increase of E_{CB} of the semiconductor, tuning E_A to a lower energy level, reducing the density of electron trap states (N_S) and the recombination rate (k_{rec}). In the following sections, we will focus the discussion on the improvements of V_{OC} by the development of redox shuttles

that have lower E_A than I^-/I_3^- and the passivation of the semiconductor surface which can decrease the diode saturation current and increase the shunt resistance.

2.2.1 Tuning the potential of the redox shuttles. As shown in Fig. 1, V_{OC} is thermodynamically determined by the difference between the electron quasi-Fermi level (QFL) in the TiO_2 film under illumination condition and the redox potential of the redox couple in the electrolyte. The typical redox couple used in DSCs is the combination of I^-/I_3^- because of its suitable oxidation/reduction potential, slow recombination reaction, excellent solubility, and ionic mobility in organic solvents. However, a large over-potential is needed for efficient dye regeneration owing to the formation of the intermediate I_2^-. Therefore, the development of new redox shuttles, with lower potential and enough driving force for efficient dye regeneration, is one of the major methods to further enhance V_{OC}.

As alternatives to I^-/I_3^-, other redox shuttles such as transition metal mediators of ferrocene/ferrocenium,[169] copper(I)/(II) complexes,[170] Ni(III)/Ni(IV) bis(dicarbollide),[171] with good solubility and redox properties have been studied and reviewed.[172,173] The lower redox potential, for example, ferrocene/ferrocenium improves V_{OC} value up to 0.842 V with total device efficiency of 7.5%. The Co-polypyridyl complexes have more positive redox potentials between Co(II)/Co(III) couples than that of I^-/I_3^- couple, which can provide a high V_{OC} value of over 1 V (Fig. 16).[174–176] However, no successful result in the DSCs has been reported for a long time due to the slow mass transport in the electrolyte and quick recombination between electrons and Co redox compared with the iodide.[174,175] In 2010, $[Co(bpy)_3]$ complex based redox mediator was reported to achieve a high V_{OC} value of 0.92 V and a conversion efficiency of 6.7% by using sterically hindered D35 organic sensitizer.[177] In this study, three key factors enabling to achieve high efficiency using with Co redox shuttle were revealed. First, the introduction of a number of long alkyl chains into dye molecule effectively separates the Co complex from TiO_2 surface in order to prevent the charge recombination. Second, thinner TiO_2 film less than 10 μm was employed to decrease transport length of Co redox. Third, use of small Co redox mediator consisting of pristine bpy ligand to improve the diffusion in the mesoporous TiO_2 electrode. Since this study, the $[Co(bpy)_3]$ complex was successfully used in more DSCs sensitized with sterically hindered dyes such as Y123,[178] C213,[179] M19,[180] YD2-*o*-C8,[5] with high V_{OC} values of 0.9–1.0 V and high conversion efficiencies. The relationships among alkyl chain length, configurations of the sensitizer molecules, and photovoltaic performances were further investigated.[181] Longer alkyl chains decreased the tilt angle between dye and TiO_2 substrate and inhibited charge recombination. According to these studies, both vertically and horizontally directed moderate-long alkyl (or alkoxy) chains are important to achieve high conversion efficiency with higher V_{OC} values in the Co(II/III)-complex based redox systems. Additionally, bulky truxene-based organic dyes, *e.g.* truxene-based M19 dye, do not possess long alkyl chains, but provided a high V_{OC} value of 0.9 V.[180] This is indicative that not only alkyl chains but also bulky substituents are applicable to the Co-polypydidyl system as well as aggregation-free sensitizers. Among the attempts of finding new redox complex, the current challenge is to keep the regeneration efficiency near to unit when the fairly large over-potential is reduced further for higher V_{OC}.

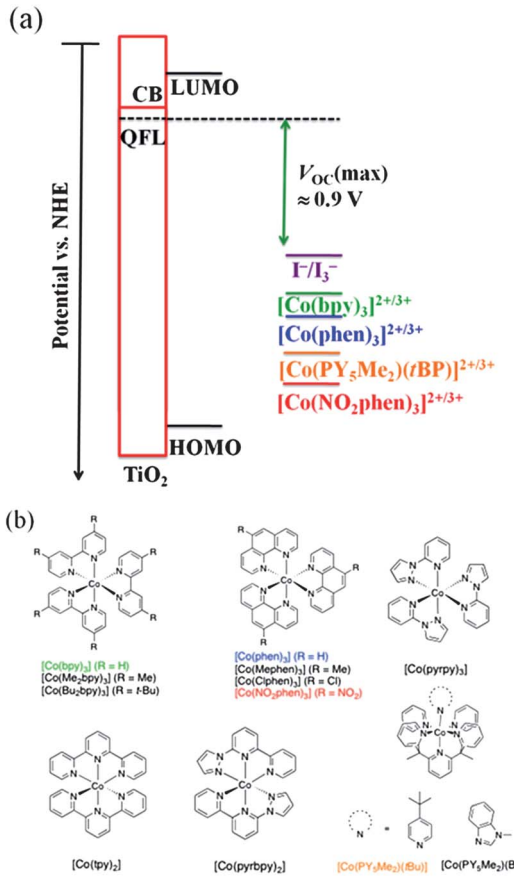

Fig. 16 (a) Energy diagram of I^-/I_3^- and some selected Co-polypyridyl redox; (b) molecular structures of selected Co-polypyridyl redox mediators.

2.2.2 Surface passivation. Surface passivation is one of the most effective methods used to increase V_{OC} by blocking the electron transfer from the semiconductor photoelectrodes to the acceptors in redox species (Fig. 17). Generally there are two methods of surface passivation: coating an inorganic ultra-thin layer or adding organic compounds in the electrolyte to form a compact molecular layer. Surface coating the semiconductor photoelectrode by another wider bandgap metal oxide, such as MgO, Al_2O_3, and SiO_2, was often employed to form a core–shell structured TiO_2 or SnO_2 photoelectrode to improve the energy conversion efficiency of DSCs.[182–188] These metal oxides acted as a blocking layer that effectively retarded the interfacial charge recombination. For example, cells using SnO_2 photoelectrode have severe recombination losses. With an ultra-thin shell of MgO on the surface of SnO_2 film, the V_{OC} of the cell significantly increased from 0.388 to 0.758 V by suppression of the electron recombination loss. In the meantime, J_{SC} was also increased from 10.74 to 14.21 mA cm^{-2} and resulted in a high improvement of conversion efficiency to 7.21%.[189] When ultra-thin MgO film was applied on the TiO_2 photoelectrode, the cell showed an increase in the V_{OC} of about 20 mV with a slight increase of J_{SC} as well and led to a conversion efficiency improvement from

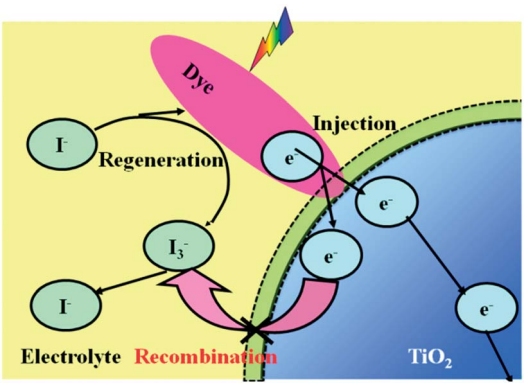

Fig. 17 Schematic pictures of the effect of surface passivation at TiO_2–dye–electrolyte interface.

6.45 to 7.57%.[188] Although coating thin metal oxides films can effectively passivate the photoelectrodes and repress the electron recombination reaction, in high efficient cells, decrease of J_{SC} is often found because this insulated layer will affect electron injection into the photoelectrode conduction band. Recently, atomic layer deposition method growing ultra-thin layers at atomic level provides a way to solve this problem. A successful example is atomic layer deposition of an ultra-thin layer of Ga_2O_3 in a few angstroms on the surface of TiO_2 film.[190] V_{OC} of 1.1 V was achieved with state-of-the-art organic D–π–A sensitizer and cobalt redox mediator. These obviously improvements suggest that coating an ultra-thin film of wider bandgap metal oxide on the photoanode is a promising method for further increasing the efficiencies of DSCs.

Compared with lots of work that had predominantly focussed on the treatment of the TiO_2 prior to the dye loading process, surface passivation of the TiO_2 film after dye adsorption provides another solution to improve both of J_{SC} and V_{OC}.[191] Recently, such post-surface passivation was developed by forming a glass-encapsulated TiO_2 surface with selective deposition of an insulating and transparent layer of silica (SiO_2) only on the open areas where no adsorbed dyes were present. The solar cell performances were improved with both of V_{OC} and J_{SC} increased at the same time.[192] It will be helpful to further improve efficiency if this kind of interfacial engineering could be applied into highly efficient DSCs.

The adsorption of organic additives on the electrode surface forming a blocking layer is also an effective way to repress the electron back reaction. The most frequently used additive in DSCs with high efficiency is 4-*tert*-butylpyridine (TBP). The V_{OC} can be significantly increased when adding TBP in the electrolyte, however, it is always companied by a decrease in J_{SC}. A higher conversion efficiency is expected if J_{SC} had no loss with a significant increase in V_{OC}, as shown in Fig. 18. Many other kinds of nitrogen-containing heterocyclic compounds, such as pyrazole derivatives, imidazole derivatives, and pyridine derivatives with varying molecular size, partial charge, and dipole moment had been investigated instead of TBP in order to eliminate the trade-off between V_{OC} and J_{SC}.[193,194] However, almost all of the additives enhanced V_{OC}, but still reduced J_{SC} (Fig. 19). Understanding the underlying mechanism of trade-off phenomena is therefore becoming very important. The trade-off has been actively studied by several methods, such as intensity modulated photovoltage spectroscopy,[14] Fourier transform infrared spectroscopy,[195] the charge extraction method,[196,197] and density functional theory calculations.[193] TBP was speculated to interacted with the semiconductor, dye, and electrolyte in the DSCs. With a three electrode DSC system,[198] we measured the QFL variation affected by TBP during the *I–V* characterization, as shown in Fig. 20. It was found that TBP can negatively shift the QFL of TiO_2 film under both short circuit and open circuit conditions and a linear relationship between the QFL shifts under these two conditions was obtained. The effect of TBP was also found to be influenced by the nature of cations in the electrolyte and the QFL of the semiconductor.[199] If the QFL shift at open circuit was much larger than the shift at short circuit by developing new additives, the trade-off is possible to be eliminated and a higher efficiency is expected.

2.3 Fill factors

Fill factor is a key parameter of a solar cell to represent the condition of the maximum power output, P_M, with corresponding current I_M and voltage V_M. It is defined as the ratio of P_M to the production of J_{SC} and V_{OC}. The operating point of P_M can be derived by differentiating the output power, $P = IV$, with respect to voltage and finding the point of derivative equal to zero. Although it is hard to get an analytical solution of this differentiating equation for further analysis of FF, the strategy to improve FF can be deduced simply from analysing the equivalent circuit given in Fig. 2. At the operating point of V_M, the current flowing into the series resistance is I_M and that flowing into the diode and shunt resistance is $I_{ph} - I_M$. Therefore, in order to get a higher FF, we should decrease the R_s to lower the energy loss in the series resistance, $P_s = I_M{}^2R_s$, and increase the R_{sh} to lower the energy loss in the shunt resistance, $P_{sh} = (V_M + I_MR_s)^2/R_{sh}$.

R_{sh} is for the resistance related to the back electron transfer across the TiO_2–dye–electrolyte interface mainly in the dye-free regions. The shunt resistance can be roughly estimated from the slope of the *I–V* curve at short circuit, which is typically of the order of $10^3\ \Omega\ cm^2$ in well-fabricated DSCs. The methods to

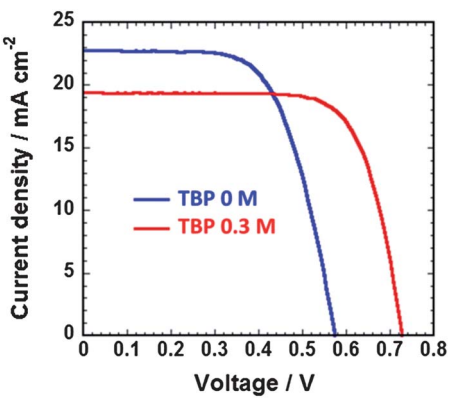

Fig. 18 *J–V* characteristics of DSCs with 0.3 M TBP and without TBP addition in the electrolyte.

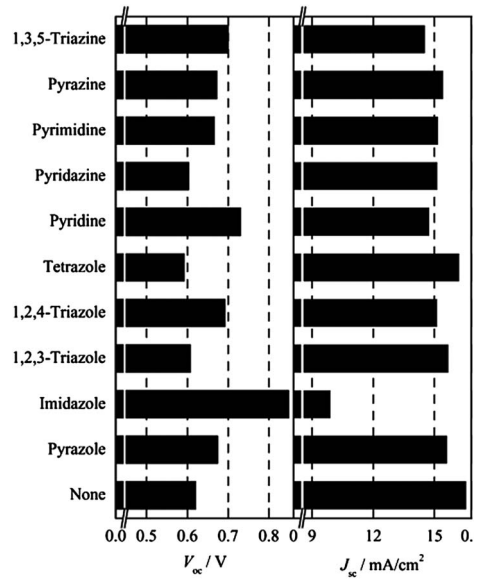

Fig. 19 The influence of some selected nitrogen-containing heterocycles in the electrolyte on the solar cell performance for a N719 dye-sensitized TiO_2 solar cell. Conditions: electrolyte, 0.6 M 1,2-dimethyl-3-propylimidazolium iodide + 0.1 M LiI + 0.05 M I_2 + 0.5 M additive in acetonitrile.[194] Reprinted from ref. 194. Copyright 2005, with permission from Elsevier.

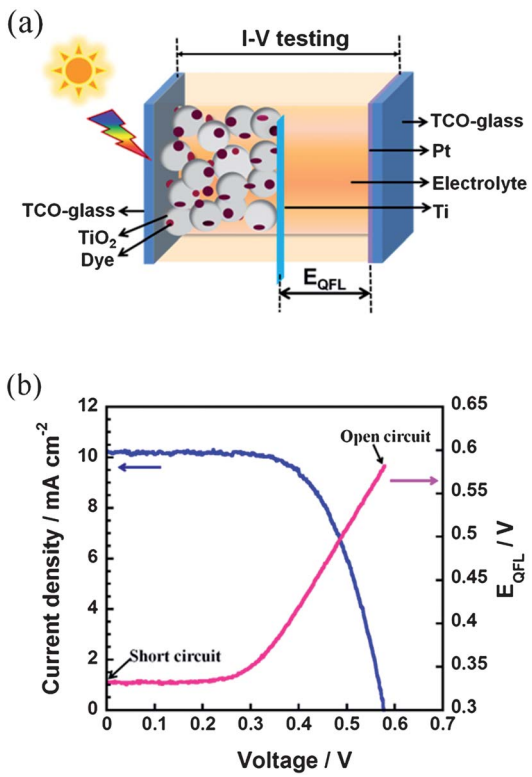

Fig. 20 (a) Schematic picture of 3-electrode DSCs and (b) the QFL of TiO_2 film variation during *J–V* measurement.[198]

increase R_{sh} are similar to those to increase V_{OC} by surface passivation of the photoelectrode. Therefore, here we will not describe them in detail.

The series resistance R_s of a DSC under direct current condition refers to the sum resistance of R_1, R_3, and R_h, and the decrease of these resistances will improve FF. R_1 is the resistance related to the charge-transfer processes occurring at the Pt counter electrodes. By systematic experiment, we confirmed that R_1 was inversely proportional to the roughness factor (RF) of the counter electrodes (Fig. 21a) and the increase of RF accelerated the reduction rate of I_3^- to I^-.[20,200] RF is related to the total surface area of the counter electrode, which can be improved by depositing the Pt thin films with larger total surface area on glass substrates or employing alternative materials with larger surface area as counter electrodes.

R_3 is related to the ion transport processes in the electrolyte and is affected by the ion transfer rate and the transport distance. Decreasing the friction between two ions or between ions and solvent molecules in the electrolyte can effectively increase the ion transfer rate. Therefore, the electrolyte solvent with low viscosity such as acetonitrile is favourable for the decrease of the R_3 value. The relationship between R_3 and the thickness of the electrolyte layer is given in Fig. 21b. It was found that cell performance can be improved by setting the counter electrode close to the TiO_2 film with a corresponding value of R_3 close to 0.7 Ω cm.[20,200]

This minimum resistance of 0.7 Ω cm is ionic diffusion resistance in porous TiO_2 film, which can be reduced by decreasing the film thickness. The combination of using a thinner TiO_2 film and dyes with higher molar extinction coefficient is a feasible way to get higher FF.

R_h is mainly attributed to the sheet resistance of the TCO substrates and experimental results showed that R_h increased in proportion to the increase of the sheet resistance of TCO.[200]

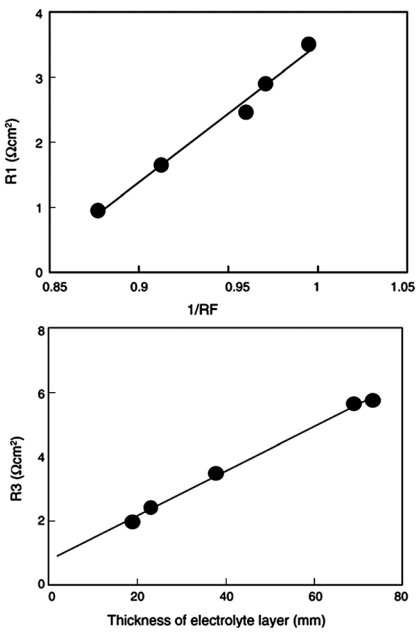

Fig. 21 (a) Dependence of R_1 on roughness factor (RF) of the counter electrodes. (b) Dependence of R_3 on thickness of electrolyte layer.[20,200] Reprinted from ref. 20. Copyright 2005, with permission from Elsevier and reprinted with permission from ref. 200. Copyright 2005, American Institute of Physics.

Theoretically, R_h could be reduced by using TCO with much low sheet resistance, however, too much of a decrease in the sheet resistance of TCO will cost the transmittance and result in a lower J_{SC}. The sheet resistance of TCO used in normal DSCs is about 10 Ω sq^{-1} and gives an R_h of about 1.0 Ω cm^2. For example, a decrease of the resistance of TCO to 5 Ω sq^{-1} correspondingly decreases the R_h to 0.5 Ω cm^2, but also reduces the transmittance at wavelength of 600 nm from 83 to 78%.

As mentioned above, the series resistance can be reduced by simultaneously increasing RF of the counter electrode materials, decreasing sheet resistance of the TCO substrate, or using a thinner electrolyte layer with low viscosity solvent. These factors should be optimized to improve the high efficiencies of DSCs. We optimized these factors and decreased R_1 to 0.4 Ω cm^2, R_3 to 0.7 Ω cm^2, and R_h to 0.7 Ω cm^2 so that the total series resistance of the cell was successfully decreased to 1.8 Ω cm^2 and FF was improved by 3%, which increased the conversion efficiency to 10.2% (Fig. 22).[200]

2.4 Back-contact dye-sensitized solar cells

In DSCs, TCO glass is used as the transparent substrate with about 20% of the incident light lost, in which 10% is reflected by the glass and the other 10% lost in the TCO layer. If the TCO layer could be omitted, a higher J_{SC} can be expected because of the increase in incident light intensity.[201] In 2007, we fabricated new structure DSCs without TCO layer and achieved an overall conversion efficiency of 7.1% (Fig. 23a).[202] In this structure, TiO_2 film is directly formed on the glass substrate and the front electrode is moved to the back side of the TiO_2 film. This structure is similar to back contacted silicon solar cells, in which the front electrode is moved to the back side in order to increase the irradiation area. Hence we named this structure as back contact dye-sensitized solar cell (BCDSC). Additionally, the back contact structure can further reduce the production cost because TCO glass is one of the most expensive materials in the DSCs.

The back contact electrode (BCE) of this structure, which fabricated on the TiO_2 film opposite to the glass substrate, must have a porous structure to pass through redox shuttle and is not

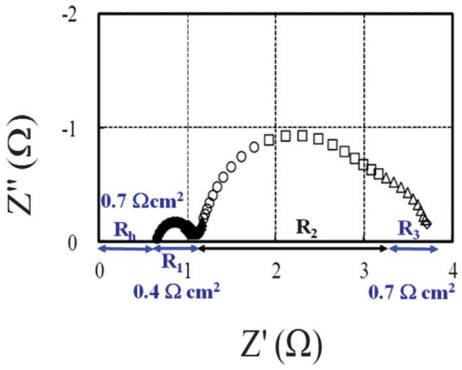

Fig. 22 Optimization of series resistance of a DSC with high efficiency, data adopted from ref. 200. Reprinted with permission from ref. 200. Copyright 2005, American Institute of Physics.

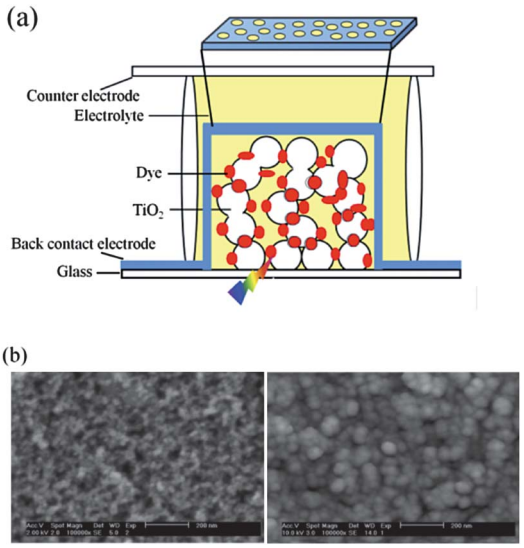

Fig. 23 (a) Schematic structure of back-contact type DSCs. (b) SEM images of TiO_2 surface (left) and BCE based on Ti metal (right).[202] Adapted from ref. 202. Copyright 2007, reprinted with permission from The Japan Society of Applied Physics.

corroded by iodide/triiodide.[203] Titanium deposited in vacuum was found to be suitable as the BCE of BCDSCs. It was also found that controlling the deposition time can adjust the porous size of the BCE. The pore size of *ca.* 10 nm is the best condition for obtaining FF of equal value as in conventional DSCs because this pore size is large enough to pass through the I_3^- ions with a molecular size of 1 nm (Fig. 23b). As a result, BCDSCs with N719 based on porous Ti–BCE obtained J_{SC} of 13.7 mA cm^{-2}, V_{OC} of 0.72 V and FF of 0.72.[204]

In order to further improve the efficiency, electrolyte diffusion behaviour in TiO_2 film was studied and it was found the electron injected into TiO_2 film in BCDSCs had to move a longer distance than conventional DSCs.[205–207] Improvement of the electron transport property in the TiO_2 film by $TiCl_4$ treatment led to an efficiency of 8.9%.[206] Other researches on BCDSCs were mainly focused on the development of materials as BCEs. ZnO, ITO, and TiN were proposed for this purpose.[208–211]

In 2010, another type of BCDSC based on microstructured interdigitated finger electrodes (MIFE) was fabricated by lithographic method (Fig. 24).[212] In this BCDSC device, both the MIFE and ITO electrode were fabricated on the same glass substrate. This structure is almost the same with back contact of silicon solar cells because electrons and holes are collected on the same side of the cell.

3 Future directions

As shown in Table 1, we summarized the published results of certified highly efficient DSCs with efficiencies over 10% under standard conditions by public test centres.[4,6,20,25,213–215] To our best knowledge, in contrast to other uncertified high efficiencies, these certified efficiencies were all obtained from DSCs based on black dye. In addition, well fabricated submodules based on black dye have been reported with efficiency of up to

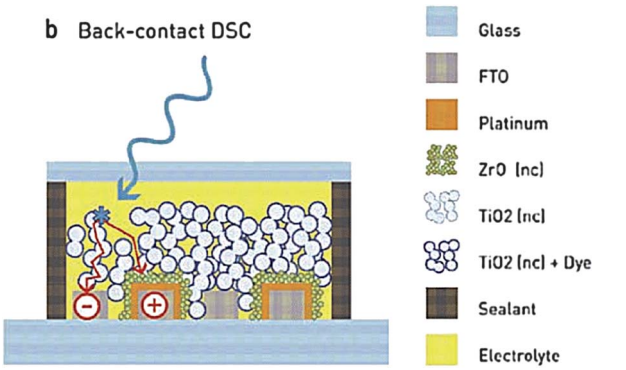

Fig. 24 Cross-sectional view of a new structured back-contact DSC.[212]

9.9% for current collection type,[9,216] and efficiency of 9.2% for integrated type. However, the present highest efficiency of DSCs is relatively low in comparison with that of 25% for bulk silicon solar cells. Therefore the efficiency of DSCs should be further improved because it is the most practical way to reduce the electricity generation cost for future commercialization.

3.1 Limitation on efficiency

Although some papers reported the theoretical efficiency is *ca.* 30%,[217] there are few chances to reach this efficiency because the energetic loss in DSCs is not fully taken into account. The theoretic maximum of output photovoltage, V_{OC}, in typical DSCs is determined by the potential difference between the conduction band bottom of semiconductor photoelectrode and the potential of the redox species in electrolyte (Fig. 1b). In the case of TiO_2 and I^-/I_3^-, this energy difference is near 0.9 V. An over-potential of 0.2 V is believed to be least for an efficient injection of electron from exited dye into the conduction band of TiO_2 film, and another *ca.* 0.3 V over-potential is estimated for the regeneration of the oxidized dye. Hence the energy gap of the dye greater than 1.4 eV can provide a sufficient driving force for the generation of high J_{SC}. Supposing 90% of the incident photons with energy larger than the energy gap are absorbed, J_{SC} of 30 mA cm^{-2} could be achieved and an energy conversion efficiency of 18% is expected to be obtained by current available technology to realize V_{OC} of 0.8 V and FF of 0.75, simultaneously. For further improvement of the efficiency, one way is to develop tandem DSCs by tuning each junction to convert UV-visible light and NIR light into charges, respectively, which can utilize high-energy photons more efficiently. Another way is to find how to reduce the over-potential for efficient charge generation in DSCs, which is a big challenge for current research and consequently more difficult to be achieved.

3.2 Our proposal for efficiency roadmap of DSCs

In contrast to the exponential increase in research efforts on DSCs, only a very limited improvement of efficiency had been obtained. This indicates most of the efforts played much role of trial-and-error and only a few effectively achieved in the improvement of the efficiency. In addition, many key issues are beyond present understandings and need deeper fundamental researches, such as how to develop efficient NIR dyes with high IPCE and V_{OC} output, how to overcome the J_{SC}–V_{OC} trade-off problems, how to construct multi-junction structures suitable to DSCs, and how to minimize the over-potential by suppressing the potential dispersion. Therefore, we anticipate two diverse directions of the future development of DSCs. As shown in Fig. 25, one approach is by trial-and-error in the search for new materials that are applicable to DSCs, which is important to accumulate more experience for efficiency improvements. This will take a very long time to improve only a little of the efficiency that has slowly increased in the past. Another approach is to carry out more fundamental research to reveal the original physical and chemical mechanisms in DSCs, especially those at the interfacial junctions of semiconductor–dye–electrolyte where the major process of energy conversion from light into electricity takes place. Insight into the nature of DSCs and deeper understanding of the fundamental mechanism are highly desired to illuminate the unknown field leading to highly efficient DSCs. The following illustrates the roadmap for future direction with several examples of challenges in improving the efficiency, such as to develop efficient NIR dyes, to overcome J_{SC}–V_{OC} trade-off, to integrate multi-junctions, and to control potential dispersions (Fig. 25). The achievements in such research topics will accelerate the progress in a more rapidly growing trend surpassing the baseline of trial-and-error approach.

The theoretic maximum of J_{SC} as a function of the energy gap and the achieved values in different kinds of excellent solar cells are given in Fig. 2a. The value of J_{SC} from DSCs based on black dye, which has an energy gap (E_g) of approximately 1.6 eV, shows a little deviation from the theoretical line. In order to

Table 1 Summary of published results of DSCs with certified efficiencies of over 10% under standard conditions by public test centres[a]

Efficiency (%)	Area (cm^2)	J_{SC} (mA cm^{-2})	V_{OC} (V)	FF	Sensitizer	Test centre	Achieved by	Year
11.4	0.231(ap)	21.34	0.743	0.722	Black dye	AIST	NIMS[6]	2011
11.1	0.219(ap)	20.90	0.736	0.722	Black dye	AIST	Sharp[4]	2006
10.9	0.203(ap)	20.80	0.744	0.704	Black dye	AIST	AIST[213]	2008
10.4	0.186(ap)	20.50	0.721	0.704	Black dye	NREL	EPFL[25]	2001
10.2	0.231(ap)	21.30	0.692	0.69	Black dye	AIST	TUS[214]	2006
10.9	1.094(ap)	22.20	0.732	0.673	Black dye	AIST	NIMS[215]	2012

[a] (ap): aperture area.

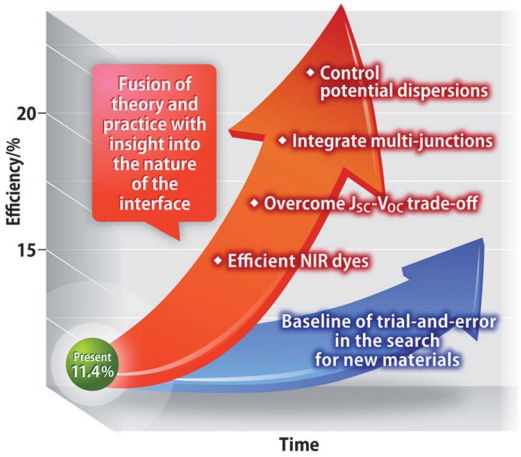

Fig. 25 Our proposal for efficiency roadmap of DSCs.

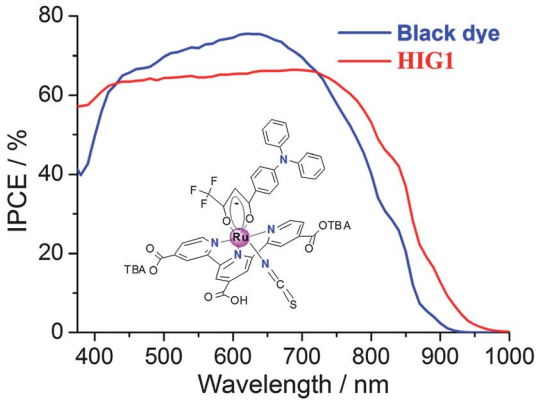

Fig. 26 IPCE spectra of DSCs based on black dye and HIG1.[218] Adapted from ref. 218, Copyright 2010, reprinted with permission from The Japan Society of Applied Physics.

achieve a higher efficiency, new NIR dyes with a narrower energy gap than black dye are expected to generate greater J_{SC}. This may be more easily realized for organic chemists because many NIR dyes for photo-recording materials have already been commercialized. However, up to now only black dye sensitized solar cells which have an IPCE spectrum extending to 850 nm possessed relatively high values of J_{SC} and V_{OC} so that the certified efficiencies of over 10% listed in Table 1 were all obtained by using black dye. Other ruthenium dyes, for example HIG1 dye which was composed of two thiocyanatos and β-diketonato derivatives, extended the IPCE spectrum to 900 nm, but the IPCE in the visible region decreased and the V_{OC} also decreased with consequent low energy conversion efficiency (Fig. 26).[218] In the case of organic dyes with high IPCE spectra, the sensitized wavelength region is *ca.* 100 nm narrower than that of black dye. Extending the IPCE spectrum to the longer wavelength region will also decrease the value in the visible region. Hence future research should elucidate the reason why IPCE and V_{OC} are decreased when extending the IPCE of NIR Ru dyes and organic dyes to the longer wavelength region than that of black dye. One hypothesis to interpret the above issues is that at the interfacial junctions of semiconductor–dye–electrolyte, the adsorption states of dyes on TiO_2 surface can affect the efficiency of charge generation and recombination.[219] Thus, the direct observation of the adsorption states of dyes is desired in the study of its correlation to the device performance. For example we successfully observed two distinct adsorption morphologies of black dyes on TiO_2 single crystal by scanning tunnelling microscope (STM) measurement and found the dyes are aggregated and adsorbed on the TiO_2 [001] surface without DCA, while the dyes are isolated when using DCA, as shown in Fig. 27.[220] We expected more detailed observation of the adsorption states of dyes and additives on the semiconductor surface, which will be very helpful to investigate the electronic process at the interfacial junctions of semiconductor–dye–electrolyte.

As discussed in Section 2.2.2, the increase of V_{OC} was always accompanied with a decrease of J_{SC} when the TiO_2 surface is passivated by additives of nitrogen-containing heterocyclic compounds in the electrolyte, while in silicon solar cells, the surface passivation does not induce such a J_{SC}–V_{OC} trade-off. If this trade-off problem in DSCs could be solved, the efficiency can be improved by 20–30%. Hence, deeper understanding of the underlying mechanism of passivation at the interfacial junctions of semiconductor–dye–electrolyte in DSCs is very important to solve this trade-off. For example as discussed in Section 2.2.2, we found linear relationships between the QFL shifts at short circuit and open circuit.[199] The slope of the line is equal to or less than 1 depending on the cation species in the electrolyte, as shown in Fig. 28. If the slope would be larger than 1, the QFL shift at open circuit would be much larger than the shift at short circuit and the trade-off between J_{SC} and V_{OC} might be solved to obtain higher efficiency DSCs. Recently, we also revealed a new factor affecting the J_{SC}–V_{OC} trade-off by the formation of a hydrogen bond between 4-*tert*-butylpyridine and N3 dye molecules.[221] Hence, we expected more fundamental research on the interface of the semiconductor–dye–electrolyte to solve the J_{SC}–V_{OC} trade-off. Combined with the development of new NIR dyes or new redox shuttle, the efficiency will be improved to 15% in the near future.

A tandem structure is commonly used in solar cells to increase the efficiency. Until now, tandem DSCs based on black

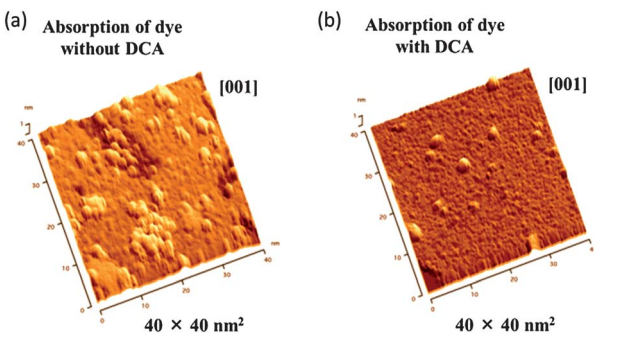

Fig. 27 STM imagines of TiO_2 [001] surface with (a) aggregated and (b) isolated black dyes, respectively.[220] Reprinted with permission from ref 220. Copyright 2008 American Chemical Society.

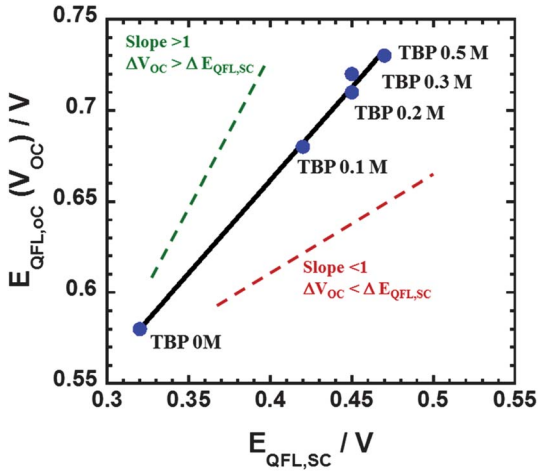

Fig. 28 Linear relationships between the QFL under short circuit and open circuit conditions with different slopes.

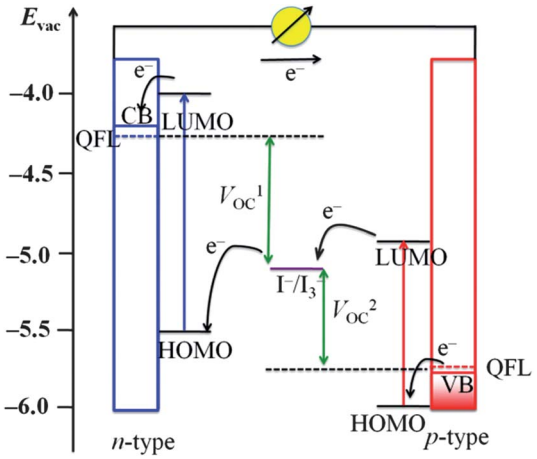

Fig. 29 Schematic drawing of the energy diagram and electron transfer process in p–n sandwich cells.

dye and N719 dye had successfully obtained efficiency of over 10%.[213,222,223] However, the efficiency of tandem DSCs is still lower than that of a single cell based on black dye. The reason is these tandem DSCs were built by two separated cells because TiO_2 film should be sintered at 500 °C. Hence, the semi-transparent counter electrode of the front cell and the TCO glass of the bottom cell will induce a loss of incident light and restrict the efficiency. In contrast, p–n sandwich DSC structures, which were proposed a long time ago, provided a promising solution because of omission of the glass sheet separator and counter electrode.[224] Unfortunately, until now, only very poor performances have been achieved owing to the very low photocurrent generated at the side of p-type photoelectrode usually composed of NiO. In such p–n sandwich DSCs, high V_{OC} would be expected if the energy level of the valence band of the p-type photoelectrode could be low enough. As shown in Fig. 29, one rational design of highly efficient p–n sandwich DSCs is to develop new p-type photoelectrodes with the valence band lower than −5.8 V (*vs.* vacuum) which will enable an output of V_{OC} of 1.35 V (0.75 V at n-side and 0.6 V at p-side), and develop new dyes with the HOMO lower than −6.0 V (*vs.* vacuum) and an energy gap of 1.1 eV to generate a J_{SC} of over 20 mA cm^{-2} at the p-type photoelectrode. Thus an overall conversion efficiency of up to 20% can be achieved with FF of 0.75 by the development of a high quality p-type photoelectrode, new dyes and light managing technology to match the photocurrents at both sides.

For higher efficiency of over 20%, the large loss-in-potential in present DSCs, which is estimated to be at least 0.5 V, with 0.2 V over-potential for efficient electron injection and another 0.3 V over-potential for the regeneration of oxidized dyes, should be minimized. This large loss-in-potential is mainly due to the potential dispersion in the materials of TiO_2, dyes, and redox shuttles. Hence, the most promising way to significantly enhance the efficiency is to develop new materials with less potential dispersion, such as nano-crystalline TiO_2 particles with only one crystallographic plane exposed for dye adsorption by which the potential dispersion of conduction bands of different planes will be reduced, new NIR dyes with rigid structure to decrease the dispersion of vibrational energy of the dyes, and redox shuttles with less derivatives to lower the dispersion in redox potentials. If the loss-in-potential is reduced to less than 0.2 V, we will obtain a much wider IPCE spectrum and higher V_{OC} simultaneously. Therefore, we expect the long term goal to improve the DSCs efficiency to over 20%, as high as that of the champion efficiency of crystalline silicon solar cells, can be achieved when all the aforementioned issues are solved. However, this will be very hard to achieve because it requires deeper fundamental researches and application of new concepts. We hope more young scientists with different backgrounds will courageously accept these challenges.

Conclusions

One of the most important keys to the future commercialization of DSCs is to further improve the low energy conversion efficiency. In this perspective article, we selectively review the major progress of improving the efficiency which may be useful for future applications in DSCs. Based on the analysis of device performance by equivalent circuit modelling, we highlight some approaches to improve the efficiency, such as extending spectral response into the near infrared region, the enhancement of the output photovoltage by tuning potentials and strengthened surface passivation, and saving energy loss by reducing series resistance and increasing shunt resistance. Finally we propose a roadmap for future direction, with the challenges of how to further improve the efficiency in the future and expect more applicable innovations to be achieved in academic research to accelerate the commercialization of DSCs.

Acknowledgements

We thank Dr Ashraful Islam and Dr Chuanjiang Qin for many helpful discussions. This research is supported by grants from the Core Research for Evolutional Science and Technology (CREST) of the Japan Science and Technology Agency.

References

1 B. O'Regan and M. Grätzel, *Nature*, 1991, **353**, 737–740.
2 U. Bach, D. Lupo, P. Comte, J. E. Moser, F. Weissörtel, J. Salbeck, H. Spreitzer and M. Grätzel, *Nature*, 1998, **395**, 583–585.
3 M. K. Nazeeruddin, A. Kay, I. Rodicio, R. Humphry-Baker, E. Müller, P. Liska, N. Vlachopoulos and M. Grätzel, *J. Am. Chem. Soc.*, 1993, **115**, 6382–6390.
4 Y. Chiba, A. Islam, Y. Watanabe, R. Komiya, N. Koide and L. Y. Han, *Jpn. J. Appl. Phys.*, 2006, **45**, L638–L640.
5 A. Yella, H.-W. Lee, H. N. Tsao, C. Yi, A. K. Chandiran, M. K. Nazeeruddin, E. W.-G. Diau, C.-Y. Yeh, S. M. Zakeeruddin and M. Grätzel, *Science*, 2011, **334**, 629–634.
6 L. Y. Han, A. Islam, H. Chen, C. Malapaka, B. Chiranjeevi, S. Zhang, X. Yang and M. Yanagida, *Energy Environ. Sci.*, 2012, **5**, 6057–6060.
7 S. Ardo and G. J. Meyer, *Chem. Soc. Rev.*, 2009, **38**, 115–164.
8 A. Hagfeldt, G. Boschloo, L. Sun, L. Kloo and H. Pettersson, *Chem. Rev.*, 2010, **110**, 6595–6663.
9 M. A. Green, K. Emery, Y. Hishikawa, W. Warta and E. D. Dunlop, *Prog. Photovoltaics*, 2012, **20**, 606–614.
10 L. M. Peter, *J. Phys. Chem. Lett.*, 2011, **2**, 1861–1867.
11 J. Bisquert, *J. Phys. Chem. B*, 2002, **106**, 325–333.
12 Q. Wang, S. Ito, M. Grätzel, F. Fabregat-Santiago, I. Mora-Seró, J. Bisquert, T. Bessho and H. Imai, *J. Phys. Chem. B*, 2006, **110**, 25210–25221.
13 N. G. Park, J. van de Lagemaat and A. J. Frank, *J. Phys. Chem. B*, 2000, **104**, 8989–8994.
14 G. Schlichthorl, S. Y. Huang, J. Sprague and A. J. Frank, *J. Phys. Chem. B*, 1997, **101**, 8141–8155.
15 L.-L. Li, Y.-C. Chang, H.-P. Wu and E. W.-G. Diau, *Int. Rev. Phys. Chem.*, 2012, **31**, 420–467.
16 J. Bisquert, A. Zaban, M. Greenshtein and I. Mora-Seró, *J. Am. Chem. Soc.*, 2004, **126**, 13550–13559.
17 J. Bisquert, *Phys. Chem. Chem. Phys.*, 2003, **5**, 5360–5364.
18 L. Y. Han, N. Koide, Y. Chiba and T. Mitate, *Appl. Phys. Lett.*, 2004, **84**, 2433–2435.
19 Q. Wang, J. E. Moser and M. Grätzel, *J. Phys. Chem. B*, 2005, **109**, 14945–14953.
20 N. Koide, A. Islam, Y. Chiba and L. Y. Han, *J. Photochem. Photobiol., A*, 2006, **182**, 296–305.
21 A. Islam, H. Sugihara and H. Arakawa, *J. Photochem. Photobiol., A*, 2003, **158**, 131–138.
22 G. Oskam, B. V. Bergeron, G. J. Meyer and P. C. Searson, *J. Phys. Chem. B*, 2001, **105**, 6867–6873.
23 T. Daeneke, A. J. Mozer, Y. Uemura, S. Makuta, M. Fekete, Y. Tachibana, N. Koumura, U. Bach and L. Spiccia, *J. Am. Chem. Soc.*, 2012, **134**, 16925–16928.
24 M. K. Nazeeruddin, S. M. Zakeeruddin, R. Humphry-Baker, M. Jirousek, P. Liska, N. Vlachopoulos, V. Shklover, C.-H. Fischer and M. Grätzel, *Inorg. Chem.*, 1999, **38**, 6298–6305.
25 M. K. Nazeeruddin, P. Péchy, T. Renouard, S. M. Zakeeruddin, R. Humphry-Baker, P. Comte, P. Liska, L. Cevey, E. Costa, V. Shklover, L. Spiccia, G. B. Deacon, C. A. Bignozzi and M. Grätzel, *J. Am. Chem. Soc.*, 2001, **123**, 1613–1624.
26 C. Barolo, M. K. Nazeeruddin, S. Fantacci, D. D. Censo, P. Comte, P. Liska, G. Viscardi, P. Quagliotto, F. D. Angelis, S. Ito and M. Grätzel, *Inorg. Chem.*, 2006, **45**, 4642–4653.
27 R. Argazzi, G. Larramona, C. Contado and C. A. Bignozzi, *J. Photochem. Photobiol., A*, 2004, **164**, 15–21.
28 T. Kinoshita, J. Fujisawa, J. Nakazaki, S. Uchida, T. Kubo and H. Segawa, *J. Phys. Chem. Lett.*, 2012, **3**, 394–398.
29 K.-L. Wu, S.-T. Ho, C.-C. Chou, Y.-C. Chang, H.-A. Pan, Y. Chi and P.-T. Chou, *Angew. Chem., Int. Ed.*, 2012, **51**, 5642–5646.
30 M. K. Nazeeruddin, Q. Wang, L. Cevey, V. Aranyos, P. Liska, E. Figgemeier, C. Klein, N. Hirata, S. Koops, S. A. Haque, J. R. Durrant, A. Hagfeldt, A. B. P. Lever and M. Grätzel, *Inorg. Chem.*, 2006, **45**, 787–797.
31 F. Gao, Y. Wang, D. Shi, J. Zhang, M. Wang, X. Jing, R. H. Baker, P. Wang, S. M. Zakeeruddin and M. Grätzel, *J. Am. Chem. Soc.*, 2008, **130**, 10720–10728.
32 D. Shi, N. Pootrakulchote, R. Li, J. Guo, Y. Wang, S. M. Zakeeruddin, M. Grätzel and P. Wang, *J. Phys. Chem. C*, 2008, **112**, 17046–17050.
33 F. Gao, Y. Cheng, Q. Yu, S. Liu, D. Shi, Y. Li and P. Wang, *Inorg. Chem.*, 2009, **48**, 2664–2669.
34 Q. Yu, S. Liu, M. Zhang, N. Cai, Y. Wang and P. Wang, *J. Phys. Chem. C*, 2009, **113**, 14559–14566.
35 Y. Cao, Y. Bai, Q. Yu, Y. Cheng, S. Liu, D. Shi, F. Gao and P. Wang, *J. Phys. Chem. C*, 2009, **113**, 6290–6297.
36 C.-Y. Chen, S.-J. Wu, C.-G. Wu, J.-G. Chen and K.-C. Ho, *Angew. Chem., Int. Ed.*, 2006, **45**, 5822–5825.
37 A. Islam, S. P. Singh, M. Yanagida, M. R. Karim and L. Y. Han, *Int. J. Photoenergy*, 2011, 757421.
38 B.-S. Chen, K. Chen, Y.-H. Hong, W.-H. Liu, T.-H. Li, C.-H. Lai, P.-T. Chou, Y. Chi and G.-H. Lee, *Chem. Commun.*, 2009, 5844–5846.
39 C.-C. Chou, K.-L. Wu, Y. Chi, W.-P. Hu, S. J. Yu, G.-H. Lee, C.-L. Lin and P.-T. Chou, *Angew. Chem., Int. Ed.*, 2011, **50**, 2054–2058.
40 C.-W. Hsu, S.-T. Ho, K.-L. Wu, Y. Chi, S.-H. Liu and P.-T. Chou, *Energy Environ. Sci.*, 2012, **5**, 7549–7554.
41 S.-H. Yang, K.-L. Wu, Y. Chi, Y.-M. Cheng and P.-T. Chou, *Angew. Chem., Int. Ed.*, 2011, **50**, 8270–8274.
42 K.-L. Wu, C.-H. Li, Y. Chi, J. N. Clifford, L. Cabau, E. Palomares, Y.-M. Cheng, H.-A. Pan and P.-T. Chou, *J. Am. Chem. Soc.*, 2012, **134**, 7488–7496.
43 H.-W. Lin, Y.-S. Wang, Z.-Y. Huang, Y.-M. Lin, C.-W. Chen, S.-H. Yang, K.-L. Wu, Y. Chi, S.-H. Liu and P.-T. Chou, *Phys. Chem. Chem. Phys.*, 2012, **14**, 14190–14195.
44 Y. Numata, S. P. Singh, A. Islam, M. Iwamura, A. Imai, K. Nozaki and L. Y. Han, *Adv. Funct. Mater.*, 2012, DOI: 10.1002/adfm.201202504.
45 T. Bessho, E. Yoneda, J.-H. Yum, M. Guglielmi, I. Tavernelli, H. Imai, U. Rothlisberger, M. K. Nazeeruddin and M. Grätzel, *J. Am. Chem. Soc.*, 2009, **131**, 5930–5934.
46 K.-L. Wu, W.-P. Ku, S.-W. Wang, A. Yella, Y. Chi, S.-H. Liu, P.-T. Chou, M. K. Nazeeruddin and M. Grätzel, *Adv. Funct. Mater.*, 2012, DOI: 10.1002/adfm.201201876.

47 K.-L. Wu, W.-P. Ku, J. N. Clifford, E. Palomares, S.-T. Ho, Y. Chi, S.-H. Liu, P.-T. Chou, M. K. Nazeeruddin and M. Grätzel, *Energy Environ. Sci.*, 2013, **6**, 859–870.
48 P. G. Bomben, K. C. D. Robson, B. D. Koivisto and C. P. Berlinguette, *Coord. Chem. Rev.*, 2012, **256**, 1438–1450.
49 Z. Ning and H. Tian, *Chem. Commun.*, 2009, 5483–5495.
50 Z.-S. Wang, N. Koumura, Y. Cui, M. Takahashi, H. Sekiguchi, A. Mori, T. Kubo, A. Furube and K. Hara, *Chem. Mater.*, 2008, **20**, 3993–4003.
51 T. Horiuchi, H. Miura, K. Sumioka and S. Uchida, *J. Am. Chem. Soc.*, 2004, **126**, 12218–12219.
52 S. Ito, H. Miura, S. Uchida, M. Takata, K. Sumioka, P. Liska, P. Comte, P. Péchy and M. Grätzel, *Chem. Commun.*, 2008, 5194–5196.
53 Y. Z. Wu, X. Zhang, W. Q. Li, Z. S. Wang, H. Tian and W. H. Zhu, *Adv. Energy Mater.*, 2012, **2**, 149–156.
54 K. Pei, Y. Wu, W. Wu, Q. Zhang, B. Chen, H. Tian and W. Zhu, *Chem.–Eur. J.*, 2012, **18**, 8190–8200.
55 H. Tian, X. Yang, R. Chen, Y. Pan, L. Li, A. Hagfeldt and L. Sun, *Chem. Commun.*, 2007, 3741–3743.
56 H. Tian, X. Yang, R. Chen, A. Hagfeldt and L. Sun, *Energy Environ. Sci.*, 2009, **2**, 674–677.
57 K. M. Karlsson, X. Jiang, S. K. Eriksson, E. Gabrielsson, H. Rensmo, A. Hagfeldt and L. Sun, *Chem.–Eur. J.*, 2011, **17**, 6415–6424.
58 H.-Y. Yang, Y.-S. Yen, Y.-C. Hsu, H.-H. Chou and J. T. Lin, *Org. Lett.*, 2010, **12**, 16–19.
59 Y. Numata, A. Islam, Y. Shirai and L. Han, *Chem. Commun.*, 2011, **47**, 6159.
60 Y. Numata and L. Han, *Jpn. J. Appl. Phys.*, 2012, **51**, 10NE13.
61 S.-L. Li, K.-J. Jiang, K.-F. Shao and L.-M. Yang, *Chem. Commun.*, 2006, 2792–2794.
62 S. Ito, S. M. Zakeeruddin, R. Humphry-Baker, P. Liska, R. Charvet, P. Comte, M. K. Nazeeruddin, P. Péchy, M. Takata, H. Miura, S. Uchida and M. Grätzel, *Adv. Mater.*, 2006, **18**, 1202–1205.
63 D. Kuang, S. Uchida, R. Humphry-Baker, S. M. Zakeeruddin and M. Grätzel, *Angew. Chem., Int. Ed.*, 2008, **47**, 1923–1927.
64 Y. Ooyama, S. Inoue, T. Nagano, K. Kushimoto, J. Ohshita, I. Imae, K. Komaguchi and Y. Harima, *Angew. Chem., Int. Ed.*, 2011, **50**, 7429–7433.
65 Y. Ooyama, T. Nagano, S. Inoue, I. Imae, K. Komaguchi, J. Ohshita and Y. Harima, *Chem.–Eur. J.*, 2011, **17**, 14837–14843.
66 K. Hara, M. Kurashige, S. Ito, A. Shinpo, S. Suga, K. Sayama and H. Arakawa, *Chem. Commun.*, 2003, 252–253.
67 K. Hara, T. Sato, R. Katoh, A. Furube, Y. Ohga, A. Shinpo, S. Suga, K. Sayama, H. Sugihara and H. Arakawa, *J. Phys. Chem. B*, 2003, **107**, 597–606.
68 T. Kitamura, M. Ikeda, K. Shigaki, T. Inoue, N. A. Anderson, X. Ai, T. Lian and S. Yanagida, *Chem. Mater.*, 2004, **16**, 1806–1812.
69 X. Ma, J. Hua, W. Wu, Y. Jin, F. Meng, W. Zhan and H. Tian, *Tetrahedron*, 2008, **64**, 345–350.
70 J. Song, F. Zhang, C. Li, W. Liu, B. Li, Y. Huang and Z. Bo, *J. Phys. Chem. C*, 2009, **113**, 13391–13397.
71 C. Teng, X. Yang, C. Yang, H. Tian, S. Li, X. Wang, A. Hagfeldt and L. Sun, *J. Phys. Chem. C*, 2010, **114**, 11305–11313.
72 A. Mishra, M. K. R. Fischer and P. Bäuerle, *Angew. Chem., Int. Ed.*, 2009, **48**, 2474–2499.
73 Y.-S. Yen, H.-H. Chou, Y.-C. Chen, C.-Y. Hsu and J. T. Lin, *J. Mater. Chem.*, 2012, **22**, 8734–8747.
74 D. P. Hagberg, T. Marinado, K. M. Karlsson, K. Nonomura, P. Qin, G. Boschloo, T. Brinck, A. Hagfeldt and L. Sun, *J. Org. Chem.*, 2007, **72**, 9550–9556.
75 N. Koumura, Z.-S. Wang, S. Mori, M. Miyashita, E. Suzuki and K. Hara, *J. Am. Chem. Soc.*, 2006, **128**, 14256–14257.
76 I. Jung, J. K. Lee, K. H. Song, K. Song, S. O. Kang and J. Ko, *J. Org. Chem.*, 2007, **72**, 3652–3658.
77 J. T. Lin, P.-C. Chen, Y.-S. Yen, Y.-C. Hsu, H.-H. Chou and M.-C. P. Yeh, *Org. Lett.*, 2009, **11**, 97–100.
78 S. Qu, C. Qin, A. Islam, J. Hua, H. Chen, H. Tian and L. Y. Han, *Chem.–Asian J.*, 2012, **7**, 2895–2903.
79 Q. Li, L. Lu, C. Zhong, J. Huang, Q. Huang, J. Shi, X. Jin, T. Peng, J. Qin and Z. Li, *Chem.–Eur. J.*, 2009, **15**, 9664–9668.
80 M. Hara, D. Kondo, T. Shono, Y. Kunugi and H. Aihara, *Chem. Lett.*, 2013, **42**, 140–142.
81 S. Paek, H. Choi, C. Kim, N. Cho, S. So, K. Song, M. K. Nazeeruddin and J. Ko, *Chem. Commun.*, 2011, **47**, 2874–2876.
82 W. Zeng, Y. Cao, Y. Bai, Y. Wang, Y. Shi, M. Zhang, F. Wang, C. Pan and P. Wang, *Chem. Mater.*, 2010, **22**, 1915–1925.
83 L.-Y. Lin, C.-H. Tsai, K.-T. Wong, T.-W. Huang, L. Hsieh, S.-H. Liu, H.-W. Lin, C.-C. Wu, S.-H. Chou, S.-H. Chen and A.-I. Tsai, *J. Org. Chem.*, 2010, **75**, 4778–4785.
84 H. N. Tsao, C. Yi, T. Moehl, J.-H. Yum, S. M. Zakeeruddin, M. K. Nazeeruddin and M. Grätzel, *ChemSusChem*, 2011, **4**, 591–594.
85 J.-H. Chen, C.-H. Tsai, S.-A. Wang, Y.-Y. Lin, T.-W. Huang, S.-F. Chiu, C.-C. Wu and K.-T. Wong, *J. Org. Chem.*, 2011, **76**, 8977–8985.
86 S. Qu, W. Wu, J. Hua, C. Kong, Y. Long and H. Tian, *J. Phys. Chem. C*, 2010, **114**, 1343–1349.
87 S. Qu, C. Qin, A. Islam, Y. Wu, W. Zhu, J. Hua, H. Tian and L. Han, *Chem. Commun.*, 2012, **48**, 6972–6974.
88 J.-H. Yum, T. W. Holcombe, Y. Kim, J. Yoon, K. Rakstys, M. K. Nazeeruddina and M. Grätzel, *Chem. Commun.*, 2012, **48**, 10727–10729.
89 S. Haid, M. Marszalek, A. Mishra, M. Wielopolski, J. Teuscher, J.-E. Moser, R. Humphry-Baker, S. M. Zakeeruddin, M. Grätzel and P. Bäuerle, *Adv. Funct. Mater.*, 2012, **22**, 1291–1302.
90 Y. Wu, M. Marszalek, S. M. Zakeeruddin, Q. Zhang, H. Tian, M. Grätzel and W. Zhu, *Energy Environ. Sci.*, 2012, **5**, 8261–8272.
91 Y. Cui, Y. Wu, X. Lu, X. Zhang, G. Zhou, F. B. Miapeh, W. Zhu and Z.-S. Wang, *Chem. Mater.*, 2011, **23**, 4394–4401.
92 J. Mao, F. Guo, W. Ying, W. Wu, J. Li and J. Hua, *Chem.–Asian J.*, 2012, **7**, 982–991.
93 D. P. Hagberg, J.-H. Yum, H. Lee, F. De Angelis, T. Marinado, K. M. Karlsson, R. Humphry-Baker, L. Sun,

A. Hagfeldt, M. Grätzel and M. K. Nazeeruddin, *J. Am. Chem. Soc.*, 2008, **130**, 6259–6266.
94 K. R. Justin Thomas, Y.-C. Hsu, J. T. Lin, K.-M. Lee, K.-C. Ho, C.-H. Lai, Y.-M. Cheng and P.-T. Chou, *Chem. Mater.*, 2008, **20**, 1830–1840.
95 G. Li, K.-J. Jiang, Y.-F. Li, S.-L. Li and L.-M. Yang, *J. Phys. Chem. C*, 2008, **112**, 11591–11599.
96 S. Kim, H. Choi, D. Kim, K. Song, S. O. Kanga and J. Ko, *Tetrahedron*, 2007, **63**, 9206–9212.
97 J. Hong, H. Lai, Y. Liu, C. Yuan, Y. Li, P. Liu and Q. Fang, *RSC Adv.*, 2013, **3**, 1069.
98 S. Ito, S. M. Zakeeruddin, R. Humphry-Baker, P. Liska, R. Charvet, P. Comte, M. K. Nazeeruddin, P. Péchy, M. Takata, H. Miura, S. Uchida and M. Grätzel, *Adv. Mater.*, 2006, **18**, 1202–1205.
99 S. Ito, H. Miura, S. Uchida, M. Takata, K. Sumioka, P. Liska, P. Comte, P. Péchy and M. Grätzel, *Chem. Commun.*, 2008, 5194–5196.
100 G. Zhang, H. Bala, Y. Cheng, D. Shi, X. Lv, Q. Yu and P. Wang, *Chem. Commun.*, 2009, 2198–2200.
101 H. Choi, I. Raabe, D. Kim, F. Teocoli, C. Kim, K. Song, J.-H. Yum, J. Ko, M. K. Nazeeruddin and M. Grätzel, *Chem.–Eur. J.*, 2010, **16**, 1193–1201.
102 B.-G. Kim, C.-G. Zhen, E. J. Jeong, J. Kieffer and J. Kim, *Adv. Funct. Mater.*, 2012, **22**, 1606–1612.
103 N. Cai, Y. Wang, M. Xu, Y. Fan, R. Li, M. Zhang and P. Wang, *Adv. Funct. Mater.*, 2012, DOI: 10.1002/adfm.201202562.
104 W. Zhao, Y. J. Hou, X. S. Wang, B. W. Zhang, Y. Cao, R. Yang, W. B. Wang and X. R. Xiao, *Sol. Energy Mater. Sol. Cells*, 1999, **58**, 173–183.
105 S. Alex, U. Santhosh and S. Das, *J. Photochem. Photobiol., A*, 2005, **172**, 63–71.
106 A. Burke, L. S. Mende, S. Ito and M. Grätzel, *Chem. Commun.*, 2007, 234–236.
107 J.-H. Yum, P. Walter, S. Huber, D. Rentsch, T. Geiger, F. Nüesch, F. D. Angelis, M. Grätzel and M. K. Nazeeruddin, *J. Am. Chem. Soc.*, 2007, **129**, 10320–10321.
108 T. Geiger, S. Kuster, J.-H. Yum, S.-J. Moon, M. K. Nazeeruddin, M. Grätzel and F. Nüesch, *Adv. Funct. Mater.*, 2009, **19**, 2720–2727.
109 L. Beverina, R. Ruffo, C. M. Mari, G. A. Pagani, M. Sassi, F. D. Angelis, S. Fantacci, J.-H. Yum, M. Grätzel and M. K. Nazeeruddin, *ChemSusChem*, 2009, **2**, 621–624.
110 Y. Shi, R. B. M. Hill, J.-H. Yum, A. Dualeh, S. Barlow, M. Grätzel, S. R. Marder and M. K. Nazeeruddin, *Angew. Chem., Int. Ed.*, 2011, **50**, 6619–6621.
111 A. Dualeh, J. H. Delcamp, M. K. Nazeeruddin and M. Grätzel, *Appl. Phys. Lett.*, 2012, **100**, 173512.
112 A. Ehret, L. Stuhl and M. T. Spitler, *J. Phys. Chem. B*, 2001, **105**, 9960–9965.
113 X. Chen, J. Guo, X. Peng, M. Guo, Y. Xu, L. Shi, C. Liang, L. Wang, Y. Gao, S. Sun and S. Cai, *J. Photochem. Photobiol., A*, 2005, **171**, 231–236.
114 M. Guo, P. Diao, Y.-J. Ren, F. Meng, H. Tian and S.-M. Cai, *Sol. Energy Mater. Sol. Cells*, 2005, **88**, 23–25.
115 T. Ono, T. Yamaguchi and H. Arakawa, *Sol. Energy Mater. Sol. Cells*, 2009, **93**, 831–835.
116 K. Funabiki, H. Mase, A. Hibino, N. Tanaka, N. Mizuhata, Y. Sakuragi, A. Nakashima, T. Yoshida, Y. Kubota and M. Matsui, *Energy Environ. Sci.*, 2011, **4**, 2186–2192.
117 K. Sayama, K. Hara, N. Mori, M. Satsuki, S. Suga, S. Tsukagoshi, Y. Abe, H. Sugihara and H. Arakawa, *Chem. Commun.*, 2000, 1173–1174.
118 W.-H. Zhan, W.-J. Wu, J.-L. Hua, Y.-H. Jing, F.-S. Meng and H. Tian, *Tetrahedron Lett.*, 2007, **48**, 2461–2465.
119 T. Maeda, N. Shima, T. Tsukamoto, S. Yagi and H. Nakazumi, *Synth. Met.*, 2011, **161**, 2481–2487.
120 S. Kolemen, O. A. Bozdemir, Y. Cakmak, G. Barin, S. Erten-Ela, M. Marszalek, J.-H. Yum, S. M. Zakeeruddin, M. K. Nazeeruddin, M. Grätzel and E. U. Akkaya, *Chem. Sci.*, 2011, **2**, 949–954.
121 K. Funabiki, H. Mase, Y. Saito, A. Otsuka, A. Hibino, N. Tanaka, H. Miura, Y. Himori, T. Yoshida, Y. Kubota and M. Matsui, *Org. Lett.*, 2012, **14**, 1246–1249.
122 Y. Numata, A. Islam, H. Chen and L. Y. Han, *Energy Environ. Sci.*, 2012, **5**, 8548–8552.
123 M. Victoria Martínez-Díaz, G. de la Torrea and T. Torres, *Chem. Commun.*, 2010, **46**, 7090.
124 M. J. Griffith, K. Sunahara, P. Wagner, K. Wagner, G. G. Wallace, D. L. Officer, A. Furube, R. Katoh, S. Mori and A. J. Mozer, *Chem. Commun.*, 2012, **48**, 4145.
125 L.-L. Li and E. W.-G. Diau, *Chem. Soc. Rev.*, 2013, **42**, 291.
126 W. M. Campbell, K. W. Jolley, P. Wagner, K. Wagner, P. J. Walsh, K. C. Gordon, L. Schmidt-Mende, M. K. Nazeeruddin, Q. Wang, M. Grätzel and D. L. Officer, *J. Phys. Chem. C*, 2007, **111**, 11760–11762.
127 C.-W. Lee, H.-P. Lu, C.-M. Lan, Y.-L. Huang, Y.-R. Liang, W.-N. Yen, Y.-C. Liu, Y.-S. Lin, E. W.-G. Diau and C.-Y. Yeh, *Chem.–Eur. J.*, 2009, **15**, 1403–1412.
128 M. K. Nazeeruddin, R. Humphry-Baker, M. Grätzel, D. Wöhrle, G. Schnurpfeil, G. Schneider, A. Hirth and N. Trombach, *J. Porphyrins Phthalocyanines*, 1999, **3**, 230–237.
129 J. He, A. Hagfeldt and S.-E. Lindquist, *Langmuir*, 2001, **17**, 2743–2747.
130 J. He, G. Benkö, F. Korodi, T. Polívka, R. Lomoth, B. Åkermark, L. Sun, A. Hagfeldt and V. Sundström, *J. Am. Chem. Soc.*, 2002, **124**, 4922–4932.
131 M. Yanagisawa, F. Korodi, J. Bergquist, A. Holmberg, A. Hagfeldt, B. Åkermark and L. Sun, *J. Porphyrins Phthalocyanines*, 2004, **8**, 1228–1235.
132 C.-L. Wang, C.-M. Lan, S.-H. Hong, Y.-F. Wang, T.-Y. Pan, C.-W. Chang, H.-H. Kuo, M.-Y. Kuo, E. W.-G. Diau and C.-Y. Lin, *Energy Environ. Sci.*, 2012, **5**, 6933–6940.
133 P. Y. Reddy, L. Giribabu, C. Lyness, H. J. Snaith, C. Vijaykumar, M. Chandrasekharam, M. Lakshmikantam, J.-H. Yum, K. Kalyanasundaram, M. Grätzel and M. K. Nazeeruddin, *Angew. Chem., Int. Ed.*, 2007, **46**, 373–376.
134 J.-J. Cid, J.-H. Yum, S.-R. Jang, M. K. Nazeeruddin, E. Martínez-Ferrero, E. Palomares, J. Ko, M. Grätzel and T. Torres, *Angew. Chem., Int. Ed.*, 2007, **46**, 8358–8362.

135 S. Mori, M. Nagata, Y. Nakahata, K. Yasuta, R. Goto, M. Kimura and M. Taya, *J. Am. Chem. Soc.*, 2010, **132**, 4054–4055.
136 L. M. Peter, *J. Phys. Chem. Lett.*, 2011, **2**, 1861–1867.
137 N. Robertson, *Angew. Chem., Int. Ed.*, 2008, **47**, 1012–1014.
138 H. Choi, S. Kim, S. O. Kang, J. Ko, M.-S. Kang, J. N. Clifford, A. Forneli, E. Palomares, M. K. Nazeeruddin and M. Grätzel, *Angew. Chem., Int. Ed.*, 2008, **47**, 8259–8263.
139 J.-H. Yum, E. Baranoff, S. Wenger, M. K. Nazeeruddin and M. Grätzel, *Energy Environ. Sci.*, 2011, **4**, 842–857.
140 H. Ozawa, R. Shimizu and H. Arakawa, *RSC Adv.*, 2012, **2**, 3198–3200.
141 R. Y. Ogura, S. Nakane, M. Morooka, M. Orihashi, Y. Suzuki and K. Noda, *Appl. Phys. Lett.*, 2009, **94**, 073308.
142 L. H. Nguyen, H. K. Mulmudi, D. Sabba, S. A. Kulkarni, S. K. Batabyal, K. Nonomura, M. Grätzel and S. G. Mhaisalkar, *Phys. Chem. Chem. Phys.*, 2012, **14**, 16182–16186.
143 C.-M. Lan, H.-P. Wu, T.-Y. Pan, C.-W. Chang, W.-S. Chao, C.-T. Chen, C.-L. Wang, C.-Y. Lin and E. W.-G. Diau, *Energy Environ. Sci.*, 2012, **5**, 6460–6464.
144 H. P. Wu, Z. W. Ou, T. Y. Pan, C. M. Lan, W. K. Huang, H. W. Lee, N. M. Reddy, C. T. Chen, W. S. Chao, C. Y. Yeh and E. W. G. Diau, *Energy Environ. Sci.*, 2012, **5**, 9843–9848.
145 K. Sayama, S. Tsukagoshi, T. Mori, K. Hara, Y. Ohga, A. Shinpou, Y. Abe, S. Suga and H. Arakawa, *Sol. Energy Mater. Sol. Cells*, 2003, **80**, 47–71.
146 J.-H. Yum, S.-R. Jang, P. Walter, T. Geiger, F. Nüesch, S. Kim, J. Ko, M. Grätzel and M. K. Nazeeruddin, *Chem. Commun.*, 2007, 4680–4682.
147 D. Kuang, P. Walter, F. Nüesch, S. Kim, J. Ko, P. Comte, S. M. Zakeeruddin, M. K. Nazeeruddin and M. Grätzel, *Langmuir*, 2007, **23**, 10906–10909.
148 T. Bessho, S. M. Zakeeruddin, C.-Y. Yeh, E. W.-G. Diau and M. Grätzel, *Angew. Chem., Int. Ed.*, 2010, **49**, 6646–6649.
149 C. J. Barbé, F. Arendse, P. Comte, M. Jirousek, F. Lenzmann, V. Shklover and M. Grätzel, *J. Am. Ceram. Soc.*, 1997, **80**, 3157–3171.
150 G. Rothenberger, P. Comte and M. Grätzel, *Sol. Energy Mater. Sol. Cells*, 1999, **58**, 321–336.
151 Y. Tachibana, H. Hara, K. Sayama and H. Arakawa, *Chem. Mater.*, 2002, **14**, 2527–2535.
152 P. Wang, S. M. Zakkeruddin, P. Comte, R. Charvet, R. H. Baker and M. Grätzel, *J. Phys. Chem. B*, 2003, **107**, 14336–14341.
153 Z. S. Wang, H. Kawauchi, T. Kashima and H. Arakawa, *Coord. Chem. Rev.*, 2004, **248**, 1381–1389.
154 N. Tétreault and M. Grätzel, *Energy Environ. Sci.*, 2012, **5**, 8506–8516.
155 J. Meier, J. Spitznagel, U. Kroll, C. Bucher, S. Fay, T. Moriarty and A. Shah, *Thin Solid Films*, 2004, **518**, 451–452.
156 Y. Zhao, S. Miyajima, Y. Ide, A. Yamada and M. Konagai, *Jpn. J. Appl. Phys.*, 2002, **41**, 6417–6420.
157 Y. Nasuno, M. Kondo and A. Matsuda, *Jpn. J. Appl. Phys.*, 2001, **40**, L303–L305.
158 Y. Chiba, A. Islam, R. Komiya, N. Koide and L. Y. Han, *Appl. Phys. Lett.*, 2006, **88**, 223505.
159 Q. F. Zhang, T. R. Chou, B. Russo, S. A. Jenekhe and G. Z. Cao, *Angew. Chem., Int. Ed.*, 2008, **47**, 2402–2406.
160 D. H. Chen, F. Z. Huang, Y. B. Cheng and R. A. Caruso, *Adv. Mater.*, 2009, **21**, 2206–2210.
161 Z.-H. Liu, X.-J. Su, G.-L. Hou, S. Bi, Z. Xiao and H.-P. Jia, *J. Power Sources*, 2012, **218**, 280–285.
162 Y. J. Kim, M. H. Lee, H. J. Kim, G. Lim, Y. S. Choi, N. G. Park, K. Kim and W. I. Lee, *Adv. Mater.*, 2009, **21**, 3668–3673.
163 Q. F. Zhang and G. Z. Cao, *J. Mater. Chem.*, 2011, **21**, 6769–6774.
164 C.-M. Lan, S.-E. Liu, J.-W. Shiu, J.-Y. Hu, M.-H. Lin and E. W.-G. Diau, *ACS Nano*, 2012, **6**, 10862–10873.
165 Q. Zhang, D. Myers, J. Lan, S. A. Jenekhe and G. Cao, *Phys. Chem. Chem. Phys.*, 2012, **14**, 14982–14998.
166 C.-M. Lan, S.-E. Liu, J.-W. Shiu, J.-Y. Hu, M.-H. Lin and E. W.-G. Diau, *RSC Adv.*, 2013, **3**, 559–565.
167 H.-J. Koo, Y. J. Kim, Y. H. Lee, W. I. Lee, K. Kim and N.-G. Park, *Adv. Mater.*, 2008, **20**, 195–199.
168 W. Q. Peng and L. Y. Han, *J. Mater. Chem.*, 2012, **22**, 20773–20777.
169 T. Daeneke, T.-H. Kwon, A. B. Holmes, N. W. Duffy, U. Bach and L. Spiccia, *Nat. Chem.*, 2011, 211–215.
170 S. Hattori, Y. Wada, S. Yanagida and S. Fukuzumi, *J. Am. Chem. Soc.*, 2005, **127**, 9648–9654.
171 T. C. Li, A. M. Spokoyny, C. She, O. K. Farha, C. A. Mirkin, T. J. Marks and J. T. Hupp, *J. Am. Chem. Soc.*, 2010, **132**, 4580–4582.
172 T. W. Hamann and J. W. Ondersma, *Energy Environ. Sci.*, 2011, **4**, 370–381.
173 M. K. Wang, C. Grätzel, S. M. Zakeeruddin and M. Grätzel, *Energy Environ. Sci.*, 2012, **5**, 9394–9405.
174 J. J. Nelson, T. J. Amick and C. M. Elliott, *J. Phys. Chem. C*, 2008, **112**, 18255–18263.
175 B. M. Klahr and T. W. Hamann, *J. Phys. Chem. C*, 2009, **113**, 14040–14045.
176 M. K. Kashif, J. C. Axelson, N. W. Duffy, C. M. Forsyth, C. J. Chang, J. R. Long, L. Spiccia and U. Bach, *J. Am. Chem. Soc.*, 2012, **134**, 16646–16653.
177 S. M. Feldt, E. A. Gibson, E. Gabrielsson, L. Sun, G. Boschloo and A. Hagfeldt, *J. Am. Chem. Soc.*, 2010, **132**, 16714–16724.
178 J.-H. Yum, E. Baranoff, F. Kessler, T. Moehl, S. Ahmad, T. Bessho, A. Marchioro, E. Ghadiri, J.-E. Moser, C. Yi, M. K. Nazeeruddin and M. Grätzel, *Nat. Commun.*, 2012, **3**, 631.
179 J. Liu, J. Zhang, M. Xu, D. Zhou, X. Jing and P. Wang, *Energy Environ. Sci.*, 2011, **4**, 3021–3029.
180 X. Zong, M. Liang, C. Fan, K. Tang, G. Li, Z. Sun and S. Xue, *J. Phys. Chem. C*, 2012, **116**, 11241–11250.
181 Y. Cao, N. Cai, Y. Wang, R. Li, Y. Yuan and P. Wang, *Phys. Chem. Chem. Phys.*, 2012, **14**, 8282–8286.
182 M. Grätzel, *J. Photochem. Photobiol., A*, 2004, **164**, 3–14.
183 E. Palomares, J. N. Clifford, S. A. Haque, T. Lutz and J. R. Durrant, *J. Am. Chem. Soc.*, 2003, **125**, 475–482.

184 C. Zhang, Y. Huang, Z. Huo, S. Chen and S. Dai, *J. Phys. Chem. C*, 2009, **113**, 21779–21783.
185 A. Kay and M. Grätzel, *Chem. Mater.*, 2002, **14**, 2930–2935.
186 G. R. A. Kumara, M. Okuya, K. Murakami, S. Kaneko, V. V. Jayaweera and K. Tennakone, *J. Photochem. Photobiol., A*, 2004, **164**, 183–185.
187 K. Tennakone, J. Bandara, P. K. M. Bandaranayake, G. R. A. Kumara and K. Konno, *Jpn. J. Appl. Phys.*, 2001, **40**, L732–L734.
188 S. Wu, H. Han, Q. Tai, J. Zhang, S. Xu, C. Zhou, Y. Yang, H. Hu, B. Chen, B. Sebo and X. Zhao, *Nanotechnology*, 2008, **19**, 215704–215709.
189 M. K. I. Senevirathna, P. K. D. D. P. Pitigala, E. V. A. Premalal, K. Tennakon, G. R. A. Kumara and A. Konno, *Sol. Energy Mater. Sol. Cells*, 2007, **91**, 544–547.
190 A. K. Chandiran, N. Tetreault, R. Humphry-Baker, F. Kessler, E. Baranoff, C. Yi, M. K. Nazeeruddin and M. Grätzel, *Nano Lett.*, 2012, **12**, 3941–3947.
191 R. Komiya, L. Y. Han, R. Yamanaka, A. Islam and T. Mitate, *J. Photochem. Photobiol., A*, 2004, **164**, 123–127.
192 H.-J. Son, X. Wang, C. Prasittichai, N. C. Jeong, T. Aaltonen, R. G. Gordon and J. T. Hupp, *J. Am. Chem. Soc.*, 2012, **134**, 9537–9540.
193 H. Kusama, Y. Konishi, H. Sugihara and H. Arakawa, *Sol. Energy Mater. Sol. Cells*, 2003, **80**, 167–179.
194 H. Kusama, M. Kurashige and H. Arakawa, *J. Photochem. Photobiol., A*, 2005, **169**, 169–176.
195 K. Hara, Y. Dan-oh, C. Kasada, Y. Ohga, A. Shinpo, S. Suga, K. Sayama and H. Arakawa, *Langmuir*, 2004, **20**, 4205–4210.
196 G. Boschloo, L. Haggman and A. Hagfeldt, *J. Phys. Chem. B*, 2006, **110**, 13144–13150.
197 S. E. Koops, B. C. O'Regan, P. R. F. Barnes and J. R. Durrant, *J. Am. Chem. Soc.*, 2009, **131**, 4808–4818.
198 S. Zhang, M. Yanagida, X. Yang and L. Y. Han, *Appl. Phys. Express*, 2011, **4**, 042301.
199 S. Zhang, X. Yang, K. Zhang, H. Chen, M. Yanagida and L. Y. Han, *Phys. Chem. Chem. Phys.*, 2011, **13**, 19310–19313.
200 L. Y. Han, N. Koide, Y. Chiba, A. Islam, R. Komiya, N. Fuke, A. Fukui and R. Yamanaka, *Appl. Phys. Lett.*, 2005, **86**, 213501.
201 J. M. Kroon, N. J. Bakker, H. J. P. Smit, P. Liska, K. R. Thampi, P. Wang, S. M. Zakeeruddin, M. Grätzel, A. Hinsch, S. Hore, U. Würfel, R. Sastrawan, J. R. Durrant, E. Palomares, H. Pettersson, T. Gruszecki, J. Walter, K. Skupien and G. E. Tulloch, *Progr. Photovolt.: Res. Appl.*, 2007, **15**, 1–18.
202 N. Fuke, A. Fukui, Y. Chiba, R. Komiya, R. Hamanaka and L. Y. Han, *Jpn. J. Appl. Phys.*, 2007, **46**, L420–L422.
203 N. Fuke, A. Fukui, R. Komiya, A. Islam, Y. Chiba, M. Yanagida, R. Yamanaka and L. Y. Han, *Chem. Mater.*, 2008, **20**, 4974–4979.
204 N. Fuke, A. Fukui, A. Islam, R. Komiya, R. Yamanaka, L. Y. Han and H. Harima, *J. Appl. Phys.*, 2008, **104**, 064307.
205 N. Fuke, A. Fukui, A. Islam, R. Komiya, R. Yamanaka, H. Harima and L. Y. Han, *Sol. Energy Mater. Sol. Cells*, 2009, **93**, 720–724.
206 N. Fuke, R. Katoh, A. Islam, M. Kasuya, A. Furube, A. Fukui, Y. Chiba, R. Komiya, R. Yamanaka, L. Y. Han and H. Harima, *Energy Environ. Sci.*, 2009, **2**, 1205–1209.
207 N. T. Salim, K. Zhang, S. Zhang and L. Y. Han, *Appl. Phys. Lett.*, 2012, **101**, 233905.
208 Y. Kashiwa, Y. Yoshida and S. Hayase, *Appl. Phys. Lett.*, 2008, **92**, 033308.
209 T. Beppu, Y. Kashiwa, S. Hayase, M. Kono and Y. Yamaguchi, *Jpn. J. Appl. Phys.*, 2009, **48**, 061504–061507.
210 B. Yoo, K.-J. Kim, D.-K. Lee, K. Kim, M. J. Ko, Y. H. Kim, W. M. Kim and N.-G. Park, *Opt. Express*, 2010, **18**, A395–A402.
211 B. Yoo, K.-J. Kim, Y. H. Kim, K. Kim, M. J. Ko, W. M. Kim and N.-G. Park, *J. Mater. Chem.*, 2011, **21**, 3077–3084.
212 D. Fu, X. L. Zhang, R. L. Barber and U. Bach, *Adv. Mater.*, 2010, **22**, 4270–4274.
213 M. Yanagida, N. O. Komatsuzaki, M. Kurashige, K. Sayama and H. Sugihara, *Sol. Energy Mater. Sol. Cells*, 2010, **94**, 297–302.
214 T. Yamaguchi, T. Miyabe, T. Ono and H. Arakawa, *Chem. Commun.*, 2010, **46**, 5802–5804.
215 X. Yang, M. Yanagida and L. Y. Han, *Energy Environ. Sci.*, 2013, **6**, 54–66.
216 M. Morooka, R. Ogura, M. Orihashi and M. Takenaka, *Electrochemistry*, 2009, **77**, 960–965.
217 J. He, H. Lindström, A. Hagfeldt and S.-E. Lindquist, *Sol. Energy Mater. Sol. Cells*, 2000, **62**, 265–273.
218 S. Gao, A. Islam, Y. Numata and L. Y. Han, *Appl. Phys. Express*, 2010, **3**, 062301.
219 A. Sasahara, K. Fujio, N. Koide, L. Y. Han and H. Onishi, *Surf. Sci.*, 2010, **604**, 106–110.
220 M. Ikeda, N. Koide, L. Y. Han, A. Sasahara and H. Onishi, *Langmuir*, 2008, **24**, 8056–8060.
221 K. Zhang, S. Zhang, K. Sodeyama, X. Yang, H. Chen, M. Yanagida, Y. Tateyama and L. Y. Han, *Appl. Phys. Express*, 2012, **5**, 042303.
222 T. Yamaguchi, Y. Uchida, S. Agatsuma and H. Arakawa, *Sol. Energy Mater. Sol. Cells*, 2009, **93**, 733–736.
223 M. Dürr, A. Bamedi, A. Yasuda and G. Nelles, *Appl. Phys. Lett.*, 2004, **84**, 3397–3399.
224 L. Y. Han, *US Pat.*, 6150605, 2000.

